

Effects and Models of Water Injection in an SI Engine

Haris Subasic and Joel Westling

Master of Science Thesis in Electrical Engineering
Effects and Models of Water Injection in an SI Engine

Haris Subasic and Joel Westling
LiTH-ISY-EX--18/5117--SE

Supervisor: **Xavier Llamas**
ISY, Linköpings universitet
Andreas Thomasson
ISY, Linköpings universitet
Henrik Voss
Volvo Cars
Olaf Eickel
Volvo Cars

Examiner: **Prof. Lars Eriksson**
ISY, Linköpings universitet

*Division of Vehicular Systems
Department of Electrical Engineering
Linköping University
SE-581 83 Linköping, Sweden*

Copyright © 2018 Haris Subasic and Joel Westling

Abstract

Downsizing and turbocharging is a popular combination nowadays in cars in order to decrease the fuel consumption. However, the boost pressure increases the risk of engine knock, limiting the engine in high-load operating points. In the current engines, fuel is used to cool the engine in these operating points, leading to a higher fuel consumption. Water injection is an effective method to mitigate knock and enable a more aggressive ignition. It enables the engine to produce more power and cools the exhaust, thereby protecting the turbocharger and the catalyst from wear. In this thesis, the effects of injecting water in an engine is investigated and a further development of a cylinder pressure model, with a model that takes the water into account, is presented and validated. The model can be used to estimate the cylinder pressure in several operating points.

Acknowledgments

We would like to thank our supervisors at Linköping University, Xavier Llamas Comellas and Andreas Thomasson, as well as our supervisors at Volvo Car Corporation, Henrik Voss and Olaf Eickel, for their support and guidance. We would also like to thank Tobias Lindell for helping us with the hardware in the test bench and his patience with our clumsiness. Moreover, we would like to thank Lars Eriksson and Volvo Car Corporation for the opportunity to do this master thesis.

A special thanks to all the other Master Thesis Students working in the same office as us, for all the good laughs and thrilling curve fever games.

*Linköping, June 2018
Haris Subasic and Joel Westling*

Contents

Notation	ix
1 Introduction	1
1.1 Background	1
1.2 Purpose and Goals	2
1.3 Thesis outline	2
2 Related Research	3
2.1 Mass Fraction Burned	3
2.2 Cylinder Pressure Modeling	3
2.3 Knock	4
2.4 Water Injection	5
3 Engine Testing	7
3.1 Injection Strategy	9
3.2 Injector Characteristics	9
3.3 Injector Control and Modeling	11
3.4 Description of the Tests	12
3.4.1 Engine Tests With Ignition Offset	12
3.4.2 Testing of Injection Strategies	14
3.4.3 Engine Tests With Lambda Offset	14
4 Effects of Water Injection	15
5 Modeling	27
5.1 The Four-stroke Cycle	27
5.2 In-cylinder Modeling	29
5.2.1 Compression part	29
5.2.2 Expansion part	31
5.2.3 Combustion part	32
5.2.4 Valve Model	33
5.2.5 Parameter Estimation	33
5.3 Heat Release Analysis	34

5.4	Burn Angle Model	36
5.5	Model Validation	38
6	Conclusions	43
6.1	Future Work	44
A	Algorithm to determine residual gas fraction	49
B	Ignition Offset Results	51
C	Burn Angle Model	53
	Bibliography	55

Notation

FREQUENTLY USED DEFINITIONS

Notation	Description
p	Pressure
T	Temperature
V	Volume
θ	Crank angle
m	Mass
N	Engine speed
ξ	Water-fuel ratio
Tq	Torque
q_{LHV}	Lower heating value

ABBREVIATIONS

Abbreviation	Description
BDC	Bottom Dead Center
CA	Crank Angle
DBL	Detonation Border Limit
EOC	End of Combustion
EVC	Exhaust Valve Closing
EVO	Exhaust Valve Opening
IVC	Intake Valve Closing
IVO	Intake Valve Opening
MBT	Maximum Brake Torque
MFB	Mass Fraction Burned
MFB50	The angle at which 50 % of the mass is burned
SOC	Start of Combustion
TDC	Top Dead Center
VVT	Variable Valve Timing

1

Introduction

1.1 Background

Environmental restrictions in engines are getting stricter each year. Nowadays, the driving emissions are tested in a controlled laboratory with standard driving cycles like the New European Driving Cycle (NEDC) or the American equivalent FTP-75 cycle. In a near future, laboratory tests will be complemented by a test called Real Drive Emissions (RDE), in which the car is driven in environments which better resemble real life driving, see ACEA [1].

A phenomenon that limits engine efficiency is engine knock. It occurs when the fuel ignites spontaneously outside of the flame front controlled by the spark plug. Knock could lead to severe engine damage and it can be avoided in several ways, for example by combustion phasing (postponing the ignition). A knock detection system prevents the ignition from exceeding the Detonation Border Limit (DBL), which in turn prevents the engine from running in operating points where knock is probable to occur. This leads to a less efficient ignition timing, which might be a problem in RDE tests. One solution to this problem might be water injection. The idea of injecting water is to lower the pressure and temperature in the cylinder. Potentially, it could prevent knock and enable earlier ignition, which would lead to an increased engine efficiency. Furthermore, usage of fuel enrichment can be avoided as the exhaust temperatures decrease when water is injected.

Nowadays, water injection is neither a new, nor a common technology employed in commercial cars. Nevertheless, there are some cars from the past which have had water injection systems implemented, for example, the SAAB 99. Moreover, BMW introduced water injection into their M4 GTS in 2016 with a design co-developed with BOSCH called "WaterBoost", see Brooke et al. [4].

1.2 Purpose and Goals

The main purpose of the thesis is to evaluate the effects of water injection in several engine operating points, where the probability of knock is high. The objective is to develop a model that can capture the water injection effects on cylinder pressure and combustion. It is intended to display effects on ignition timing so that better control strategies can be developed. Injection strategies such as timing and amount/frequency are to be included in the model.

Several questions that define the problem in this thesis are displayed below. Once the thesis is finished, these questions should be answered.

- Can the engine be more efficient using water injection?
- Which injection strategy is preferred in different operating points?
- How can the system be modeled?

Hopefully, by answering these questions, it can be easier to conclude whether or not water injection is a technology to invest in.

1.3 Thesis outline

Chapter 2 summarizes the research related to water injection, made by others. In chapter 3, the executed tests are described. Chapter 4 contains results from testing. The main focus is on results from when the engine is run at 1500 and 3500 rpm. Chapter 5, presents the created models and how they are developed. Parts of this chapter is used to produce the results in chapter 4. In the final chapter, the conclusions are drawn and ideas of the future of water injection are discussed.

2

Related Research

2.1 Mass Fraction Burned

A strategy to analyze the ignition efficiency is to study the mass fraction burned (MFB). The MFB curve shows the burn rate as function of the crank angle during a cycle. Research has shown, as stated in Eriksson [5], that the optimum spark ignition is obtained when 50% of the fuel mass has burned at 8-10° after TDC (ATDC).

The burn rate can be extracted from measured data, through heat-release analysis. The analysis is based on the first law of thermodynamics. A number of methods and models to describe the heat-release is presented in Klein [15], for example the Rassweiler-Withrow model. In this model, the burned mass normalized by the total mass of the charge form the MFB. Other methods include the Apparent heat-release model, Matekunas pressure ratio and Gatowski et.al. model.

A typical model used for parametrizing MFB is the Vibe function, described in Eriksson and Nielsen [7] and Heywood [12].

2.2 Cylinder Pressure Modeling

To model the effects of water injection, it is necessary to have a model of the in-cylinder pressure. An analytic cylinder pressure model is developed in Eriksson and Andersson [6]. The model consists of four parts, one of which is the gas exchange phase, where the pressures are approximated to be equal to the intake/exhaust manifold pressures. The compression and expansion processes are both modeled as polytropic processes, providing a pressure and temperature trace. The pressure traces from these two are subsequently interpolated to create the combustion part using the Vibe function. The initial pressure during the

compression stroke can be approximated as the intake manifold pressure at IVC. However, if the approximation does not give sufficiently accurate results, a model could be used instead. Both papers, Lindström [19] and Hashemzadeh Nayeri [11], give an example of how the intake manifold pressure can be modeled. More work has been done, investigating how cylinder pressure in SI Engines can be estimated. For example, Shiao and Moskwa [22] uses a single-zone dynamic model where the principal assumptions are that the temperature, pressure and cylinder charge are all uniform within the cylinders.

2.3 Knock

In order to understand the effects of knock, one has to know what knock is and how it happens. When the spark ignites the fuel mixture in the cylinder, it starts to burn in a controlled detonation. The flame starts at the ignition point and spreads out towards the cylinder walls. The detonation leads to an increase in the cylinder pressure and temperature. Consequently, the yet unburned gas pressure is increased as well. If the temperature and pressure is high enough, the unburned gas can ignite by itself, creating a second uncontrolled detonation in the cylinder. These uncontrolled detonations release energy much more rapid than a normal ignition, see Eriksson and Nielsen [7], which can result in severe engine damage.

To prevent knock from occurring, the ignition/combustion is postponed. This is executed with help of a limit on the spark angle, called Detonation Border Limit (DBL). The limit prevents the engine from running in operating points where knock is more probable to occur, for example at low speeds and high loads. Worm et al. [25] describes other methods to prevent knock, one of which is to use fuel enrichment since it lowers the temperature. One could also, for example, decrease the compression ratio, but these actions have a negative impact on the engine efficiency. Another possibility is to use a high octane fuel, but this is more expensive and a severe limitation to the customers.

Water has a high enthalpy of vaporization and when it is injected into the cylinder, it works as a coolant, see Rohit et al. [21]. Experiments have shown that the pressure in the combustion chamber is reduced with water injection, together with the exhaust temperatures, which means that the risk of engine knock is reduced, see Iacobacci et al. [14], Lezhong et al. [18], Hoppe et al. [13] and Worm et al. [25]. Research on how to analytically describe knock is carried out in e.g. Eriksson and Sivertsson [8], Heywood [12], and Ganestam [10]. A semi two-zone model can be used to track the burned and unburned temperatures in the cylinder chambers. The unburned temperature is included in the Arrhenius function, τ , to create the knock index in equation (2.1). This integral is used in the papers above as a knock model.

$$KI(\theta) = \int_{\theta_{ivc}}^{\theta} \frac{d\theta}{\tau} \quad (2.1)$$

where

$$\tau = \tau(ON, T_u(\theta), p(\theta)) \quad (2.2)$$

where ON is the octane number, T_u is the temperature of the unburned air/fuel mixture, p is the pressure and θ is the crank angle. Knock will, according to the model, occur when equation (2.1) is equal to a certain limit value, sometimes set to be 1.

Three phases are defined in the semi two-zone model - the unburned zone (IVC-SOC), the semi two-zone (SOC-EOC) and the burned zone (EOC-EVO). In the second zone, burned and unburned gas temperatures are tracked, together with an average cylinder temperature.

2.4 Water Injection

There are several experiments performed on engines with water injection that result in several interesting documented effects. However, there are differences in experimental setup and approach used in each experiment, and it is uncertain whether all of these effects will be seen with the hardware used in this thesis.

Several technical reports have shown similar results when it comes to the effects on engine out emissions. The NO_x emissions are reduced, HC emissions are increased and the CO and CO_2 emissions are similar, see Lanzafame [16], Lanzafame and Brusca [17], Rohit et al. [21], Iacobacci et al. [14], Mingrui et al. [20] and Hoppe et al. [13] for examples.

When it comes to the NO_x , studies have shown that, besides the amount of water that is injected, also the timing of the injection affects how much reduction of the emissions are achieved. The earlier the water is injected, the less water is needed. As seen in Rohit et al. [21], if the water is injected at 340 degrees before TDC (BTDC), a water-fuel ratio (defined as water mass divided by fuel mass) of 40% is needed to reduce the NO concentration from 3.0 to 0.5 ppm $\times 10^{-3}$. If the water is injected at 45° BTDC, a 100% of the fuel mass is needed. The authors have shown that the optimum SOI is 120° BTDC. With a 50% water-fuel ratio, this setting gives an efficiency increase of 3%. The major reason for this is that MFB50 can be moved closer to the optimum angle of 8° ATDC. In Bhagat et al. [2], investigations show how injection timing affects the vaporization of the water are carried out using a CFD model. It is found that earlier injection leads to better vaporization and decreased tendency of wall wetting formation.

In Fu et al. [9], experiments are performed to analyze the emission effects from water injection temperature. It is shown that a higher injection temperature leads to higher NO_x emissions and lower HC emissions. The water acts like a coolant, thus reducing the risk of knock since the temperature of the unburned gas is lowered. This enables the ignition to be closer to MBT and thereby reach a higher efficiency. As seen in Iacobacci et al. [14], Lezhong et al. [18] and Hoppe et al. [13], only injecting water lowers the indicated mean effective pressure (IMEP). But with an increased spark advance (ignition earlier BTDC), the authors have shown that the IMEP can increase by 1.5 bar using a 30% water-fuel ratio. This can allow the engines to have a higher compression ratio and higher boost pressure,

leading to more power output. It is also shown that the turbine inlet temperature is lowered, especially at higher engine speeds, because of the increase in the heat capacity of the charge in the cylinder, see Iacobacci et al. [14].

Moreover, the cooling of the air-fuel mixture leads to a more dense gas and hence more mass is trapped in the cylinder. With more air mass, more fuel mass can be burned leading to a higher power output, see Rohit et al. [21]. Experiments from Worm et al. [25] show that the exhaust temperature can be decreased as much as 200°C with water injection, which can protect the turbo from wear. Moreover, in Boretti [3] it is stated that water injection reduces the combustion chamber temperature and the inlet turbine temperature, resulting in higher power densities and better fuel conversion efficiencies. The author claims that the favorable combinations of boost pressure, spark advance and compression ratio are not possible with other technologies.

3

Engine Testing

The tests are executed on a Volvo Engine Architecture (VEA) generation 1. The VEA is a 4-cylinder, turbocharged, 2 litre petrol engine with direct fuel injection. Specifications of the engine can be seen in table 3.1, and geometrical parameters is found in table 5.1, chapter 5. The water is port injected using a module that is not originally a part of the engine. The water injectors are four BOSCH EV6 fuel injectors, connected to a water pump, which is fed with water, see figure 3.1. The water is injected once every cycle, at a certain angle. In this thesis, IVO is used as injection reference point. Mainly three tests are performed in this work. The most extensive test is the ignition offset test, described in section 3.4.1, where in different operating points, different water amounts are injected into the engine to see how the spark can be advanced. The other tests include an injection timing test, and a λ -offset test, described in sections 3.4.2 and 3.4.3 respectively.

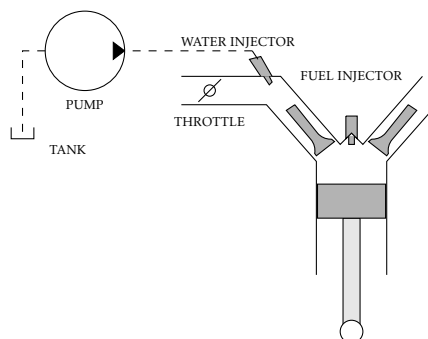


Figure 3.1: Illustration of the water injection system. The injector is fed with water from a pump, connected to a tank.

Table 3.1: Engine specifications

Engine Specifications	
Configuration	Inline 4-cylinder
Displacement	1998 cc
Bore	82 mm
Stroke	93.2 mm
Compression ratio	10.8
Fuel System	Direct injected gasoline
Induction	Single scroll turbocharged

In the tests, the engine is run in multiple operating points where the risk of knock occurrence is big. These operating points are in the high load- low speed region and in the high load- high speed region, see table 3.2. Additional operating in between are investigated as well to obtain more data. Note that ξ is the water-fuel ratio, defined as

$$\xi = \frac{m_{H_2O}}{m_f}$$

and the maximum value in the table is the maximum value tested in the engine bench. For reasons such as risk of oil dilution, which could damage the engine, a water-fuel ratio of 70 % is not exceeded.

Table 3.2: The operating points in which the engine is run during the tests. Note that FG stands for full gas.

Engine speed	Engine load (air flow)	Max. ξ [%]
1500 rpm	1.5 g/rev	70
1500 rpm	2.30 g/rev (FG)	70
2000 rpm	1.5 g/rev	70
2000 rpm	2.26 g/rev (FG)	70
2500 rpm	1.5 g/rev	60
2500 rpm	2.28 g/rev (FG)	60
3000 rpm	1.5 g/rev	60
3000 rpm	2.24 g/rev (FG)	60
3500 rpm	1.5 g/rev	60
3500 rpm	2.19 g/rev (FG)	60
4000 rpm	1.5 g/rev	40
4000 rpm	2.02 g/rev (FG)	40
4500 rpm	1.96 g/rev (FG)	40

3.1 Injection Strategy

The general strategy is to inject water while the inlet valve is open. The inlet valve is always open during an interval of 227° degrees. However, there is a window of 50° when the valve might open. The timing of the valve opening can be described by

$$IVO = IVO_{max} - iVVT \quad (3.1)$$

Where IVO_{max} is the latest point at which the valve can be opened (14.5° ATDC) and $iVVT$ is the number of degrees the opening is shifting and hence has a value between 0 and 50. Since the valve is open for a certain amount of degrees, the amount of time it is open will vary with the engine speed and is described by the following equation

$$t = \frac{60}{N} \cdot \frac{227}{360} \quad (3.2)$$

where t is the time in seconds and N is the engine speed in rpm. This means that with higher engine speed, the smaller the window of injection gets. Therefore, the number of different injection timings and the amount of water injected is reduced with higher engine speed.

3.2 Injector Characteristics

To evaluate how much water that can be injected in the different operating points, the characteristics of the injector is determined. By injecting water into a measuring cylinder during different times, a relationship between injected water mass and injection time is found. Figure 3.2 shows the water flow with different opening times at 3.2 bar pressure difference.

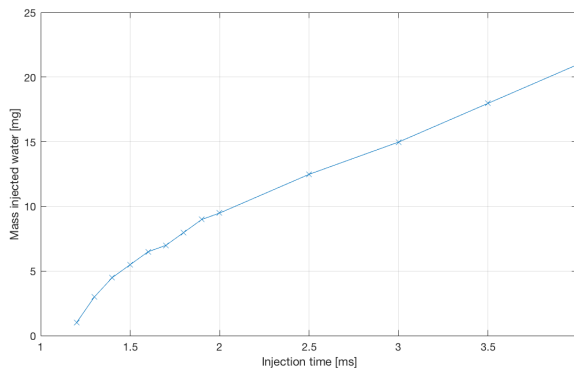


Figure 3.2: The relationship between injector opening time and water mass injected.

With the data from figure 3.2, one can calculate how much water that can be injected with equation 3.2. The result is presented in 3.3. Figure 3.4 shows

the minimum and maximum water-fuel ratio that can be used if injection is performed during IVO. For engine speeds above 1500 rpm, at least about 4 % must be injected because of the time delay which can be seen in figure 3.2. Theoretically seen, it is possible to inject more water for engine speeds below 4000 rpm, compared to the maximum amount tested in this thesis.

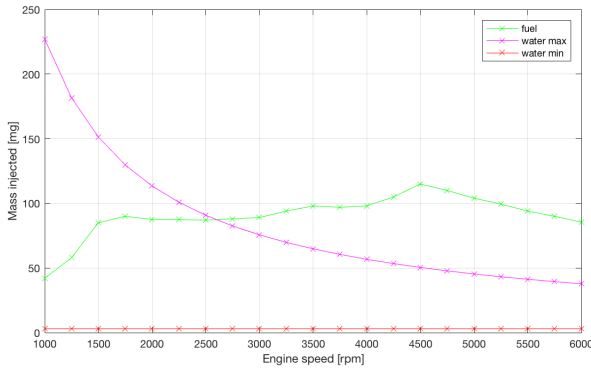


Figure 3.3: Minimum and maximum water amount at different engine speeds. The green curve shows the amount of fuel injected at maximum load.

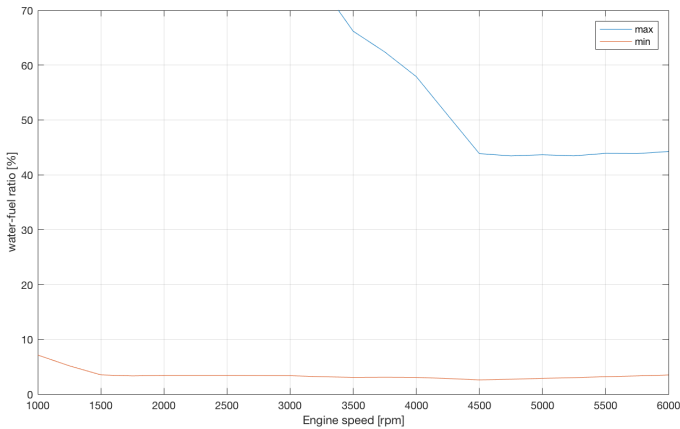


Figure 3.4: Minimum and maximum water-fuel ratio at different engine speeds.

3.3 Injector Control and Modeling

Figure 3.5 shows the Simulink block used to calculate the time of injection. The input signals are air mass flow and engine speed, together with the desired water-fuel ratio. In the tests, a look-up table is used to interpolate the injection time from a certain water mass. The values used are the ones obtained from the test of the injector characteristics. Instead of the look-up table, it is possible to use a

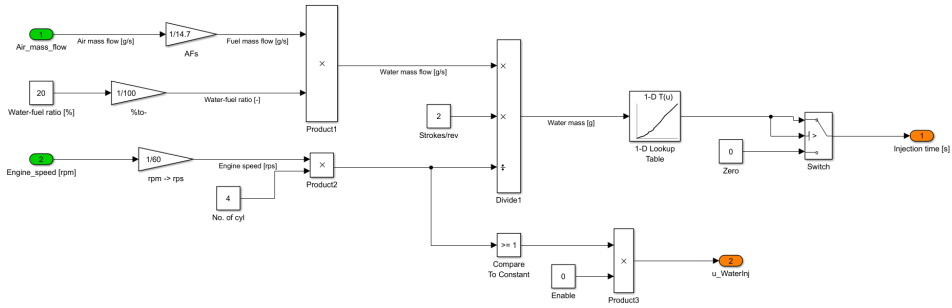


Figure 3.5: Simulink control block, where the injection time is calculated from the engine speed, air mass flow and the desired water-fuel ratio.

model to determine the injection time. Two models were created to describe the behavior in figure 3.2. The first is a fuel injection model used in Eriksson and Nielsen [7], where the fuel amount is assumed to be proportional to the injection time and the square root of the pressure difference between the injector and the pressure source. Rewritten as a water injector, the water mass injected can be expressed as

$$m_{H_2O} = c_0 \sqrt{\rho_{H_2O} \cdot \Delta p} \cdot (t_{inj} - t_0) \quad (3.3)$$

where ρ_{H_2O} is the water density, c_0 is a tuning parameter and t_0 the injection delay.

Additionally, a second order polynomial model was created. The two models, in relationship to the measured data, are displayed in figure 3.6. However, as seen in figure 3.7, the error is quite large for both lower and higher times of injection. Because of this, the 1D look-up table is used in the injector control.

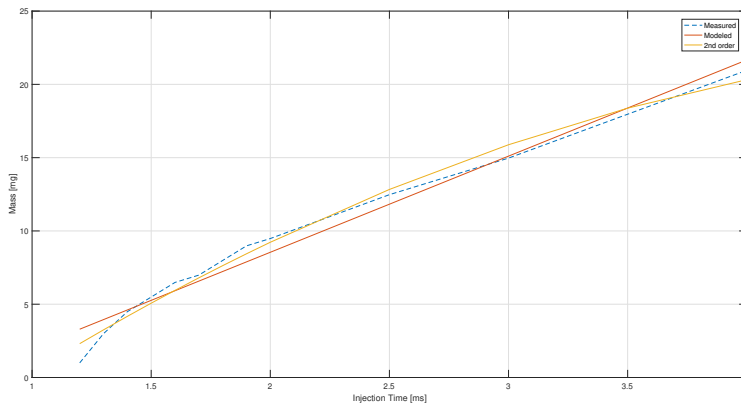


Figure 3.6: The two models in relation to measured water mass.

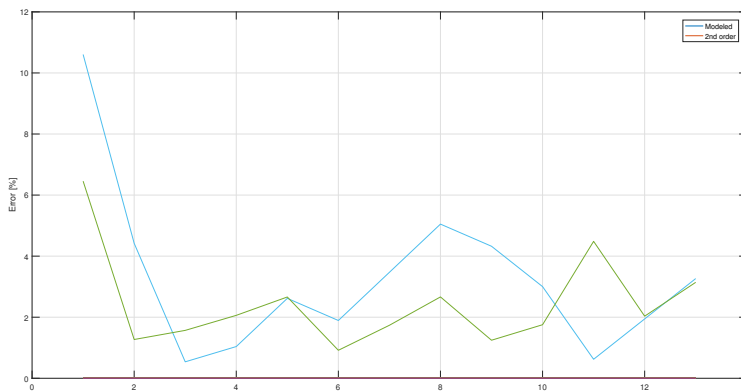


Figure 3.7: Absolute error between the models and the measured water mass.

3.4 Description of the Tests

Below, the three main tests executed in this thesis are described in detail.

3.4.1 Engine Tests With Ignition Offset

Different amounts of water is injected in different operating points. After reaching steady state for the testing point, i.e. for every fixed engine speed, torque, water amount and injection timing, the spark is manually advanced until the ac-

tive knock control is activated. This shows how much the ignition timing can be advanced when injecting a certain amount of water.

Execution

- Lock engine speed and load (air flow)
- Run the engine until it is in steady state
- Choose water amount and timing
- Inject water
- Reach steady state
- Save the data in a file
- Lock λ
- Advance the ignition until the active knock control is activated
- Document how many degrees the ignition was advanced
- Save the data in a file
- Repeat

Interesting test data to analyze include pressures, temperatures and other parameters which influence the combustion. In order to gain this information, the parameters in table 3.3 need to be recorded and saved. Note that the active knock control uses a knock detection sensor to detect knock. When it does, the ignition is postponed to protect the engine.

Table 3.3: Important parameters that will be recorded and saved during the tests.

Parameters of interest	
Cylinder pressure	P_{cyl}
Intake manifold pressure	P_{im}
Exhaust manifold pressure	P_{em}
Crank Angle	θ
Ignition angle	θ_{ign}
Exhaust temp.	T_{exh}
λ -value	λ

3.4.2 Testing of Injection Strategies

Tests are done to determine how injection timing is affecting the results. The hypothesis is that the water will cool the engine more efficiently by cooling the inlet valve before it opens. This test is only executed in one operating point (1500 rpm, FG), since all of the water can be injected before the inlet valve opens at low speed. The setup and execution is the same as in test 1. The injection timing can be seen in table 3.4

Table 3.4: Water injection timing

Test	Timing [ATDC]
1	IVO
2	IVO - 50
3	IVO - 100

3.4.3 Engine Tests With Lambda Offset

A way to improve both the fuel economy and emissions is to cool the engine with water instead of fuel. In this test, instead of advancing the ignition, λ is gradually increased until right before the active knock control is activated or until a λ -value of 1 is reached.

Execution

- Lock engine speed and load
- Run the engine until it is in steady state
- Choose water amount and timing
- Inject water
- Reach steady state
- Save the data in a file
- Increase the lambda value until the active knock control is activated
- Document how big the increase is
- Save the data in a file
- If $\lambda < 1$, repeat, if $\lambda = 1$, stop

4

Effects of Water Injection

Figures 4.1-4.4 show how the cylinder pressure changes in Cylinder 1 with different water-fuel ratios without spark advance, in four different operating points. The pressure curves are mean values from multiple cycles, obtained from measurements. The pressure peak drops as the water-fuel ratio increases, which enables the ignition to be advanced since the engine is now working further away from the knock limit. However, at some few points, the pressure increases with increased water amount. Why this happens is not entirely clear but it might happen because of some sort of measurement error.

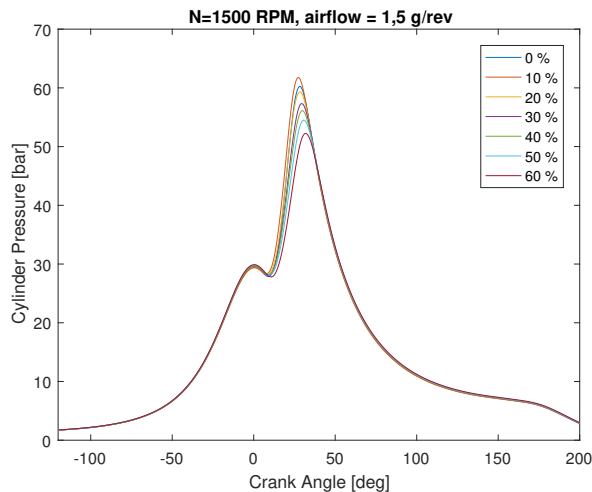


Figure 4.1: Engine speed $N = 3500$ RPM, load $m = 1.5$ g/rev

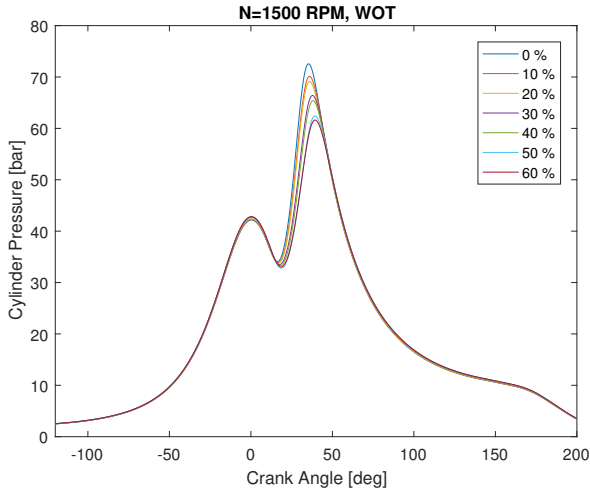


Figure 4.2: Engine speed $N = 3500$ RPM, full load

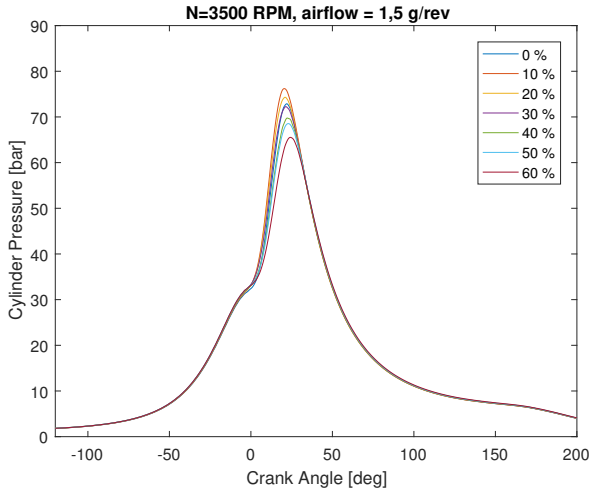


Figure 4.3: Engine speed $N = 3500$ RPM, load $m = 1.5$ g/rev

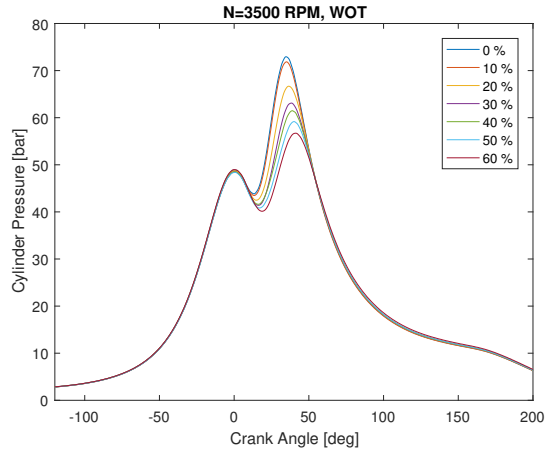


Figure 4.4: Engine speed $N = 3500$ RPM, full load

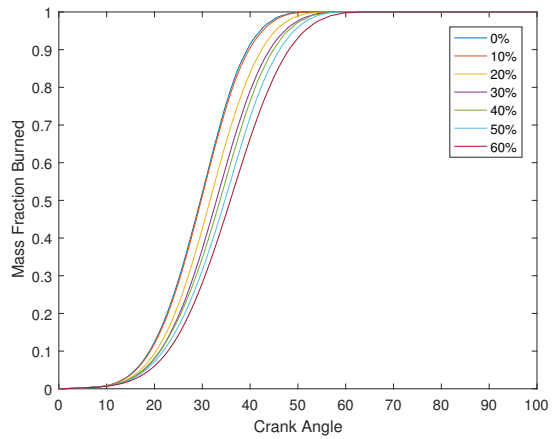
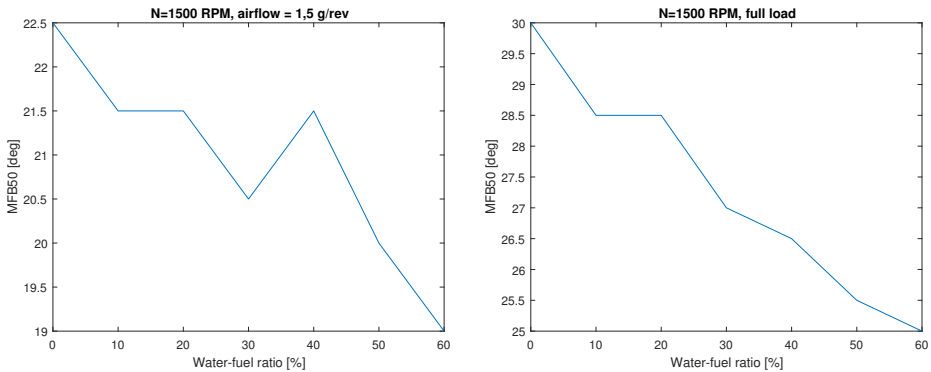
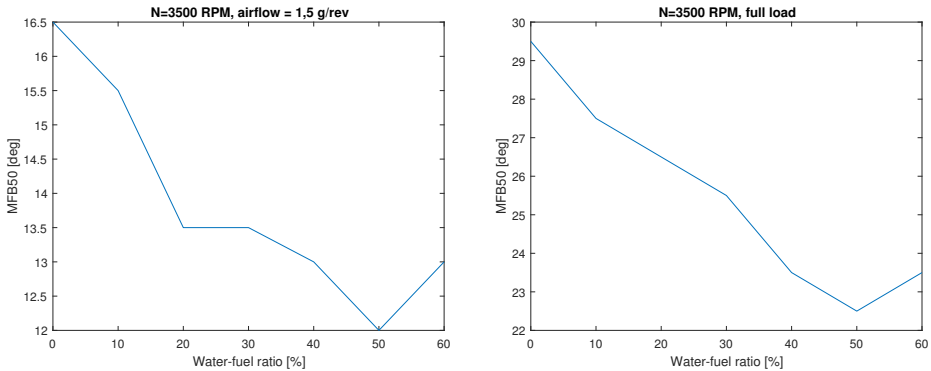


Figure 4.5: Engine speed $N = 3500$ RPM, full load

Figure 4.5 shows the mass fraction burned from the thermodynamic heat release analysis, described in chapter 5. Since the ignition angle is constant (in this case 0°), the plot clearly shows that the combustion process becomes slower with higher amounts of water injected. Moreover, MFB50, the crank angle at which 50 % of the fuel is burned, is moved away from its optimum when injecting water. This means that just water injection, with no other modification to the engine setting, will not increase the engine efficiency. However, since the pressure drop enables the spark to be advanced, this is also done when analyzing MFB50. The change in MFB50 with ignition offset is displayed in figures 4.6a-d. With more water, MFB50 is moved closer to the optimum MFB50 which is usually located at around $8-10^\circ$ ATDC.



(a) Engine speed $N = 1500$ RPM, load $m = 1.5$ g/rev (b) Engine speed $N = 1500$ RPM, full load



(c) Engine speed $N = 3500$ RPM, load $m = 1.5$ g/rev (d) Engine speed $N = 3500$ RPM, full load

Figure 4.6: MFB50 at different water amounts in different operating points

Another interesting analysis is to see how the output engine power changes with water injection. The power can be calculated from the work, which is represented by the area of the pV diagram. If the pressure and engine speed are

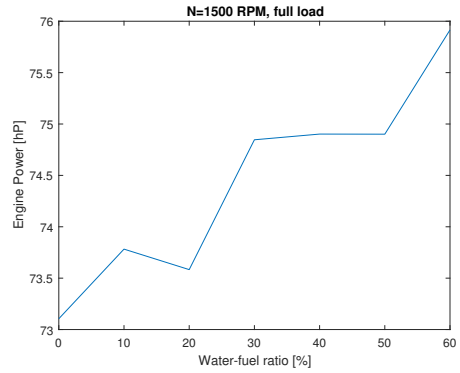
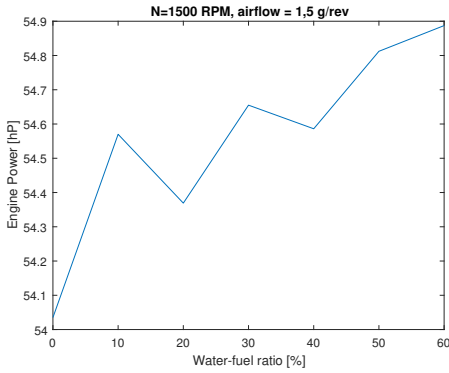
known, the power, in Watts, can be expressed

$$P_{engine} = \frac{W_{engine}}{n_r} \cdot \frac{N}{60} = \frac{N}{60n_r} \int_{-2\pi}^{2\pi} p dV \quad (4.1)$$

where n_r is the number of strokes per revolution ($n_r = 2$ for a 4 stroke engine) and W_{engine} is the engine work produced during a cycle. If equation (4.1) is divided by 735, the unit will be horsepowers [hp]. Figures 4.7a-d show the engine horsepower for different water-fuel ratios with the maximum possible ignition offset. The power, as displayed in the figures, increases with more water. The percentage power gain can be seen in Table 4.1. It is seen that the power can be more increased at high loads. Note that the engine power, in horsepowers, also can be calculated as

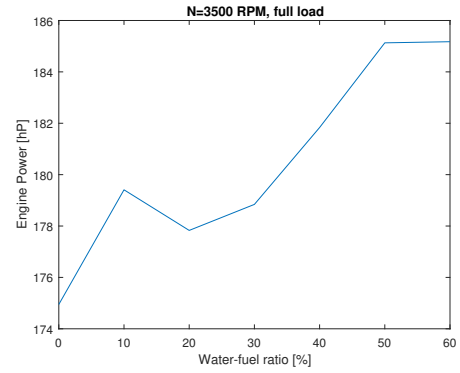
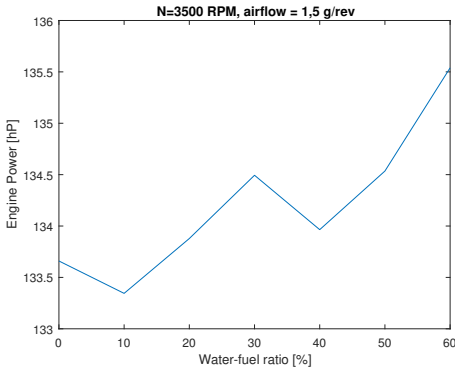
$$P_{engine} = Tq \cdot \omega_{engine} = Tq \cdot \frac{2\pi N}{60 \cdot 735}$$

which would lead to the same conclusions, i.e. the curves look the same. Only a stationary error between the two curves is obtained and it cannot be said whether the pressure sensors, used to calculate the power in equation 4.1, or torque sensor, used in the expression above, are more accurate. However, since the percentage power gain are equal in both cases, either one can be used. By comparing the MFB50- and power plots in each operating point, it is indicated that more power is obtained when MFB50 is more advanced, just as expected. When advancing the ignition, a higher pressure peak is obtained once again. The power increase comes from the fact that the pV diagram area increase is larger compared to the pV diagram decrease from the resulting slower combustion process. The combustion and its connection to efficiency will be discussed later in this chapter. As stated in chapter 3, the ignition offset is manually set until right before the Active Knock Control is activated when water is injected into the system. However, at some times during the test process, the Active Knock Control spontaneously was activated during data collection. Consequently, the spark was retarded, which explains why the power decreases and MFB50 increases between some percentages of water. Figure 4.8 shows that the Active Knock Control is activated when injecting a water amount of $\xi = 40\%$ at 3500 RPM and 1.5 g/rev.



(a) Engine speed $N = 1500$ RPM, load $m = 1.5$ g/rev

(b) Engine speed $N = 1500$ RPM, full load



(c) Engine speed $N = 3500$ RPM, load $m = 1.5$ g/rev

(d) Engine speed $N = 3500$ RPM, full load

Figure 4.7: Engine power for different water-fuel ratios with an ignition off-set.

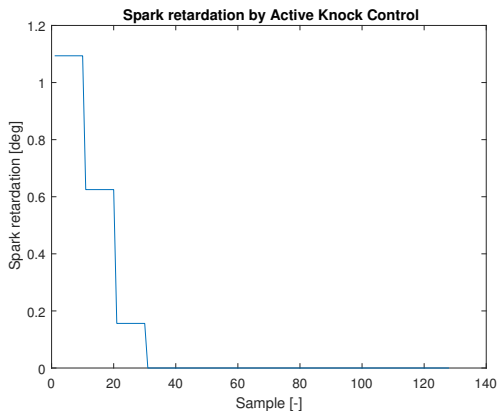
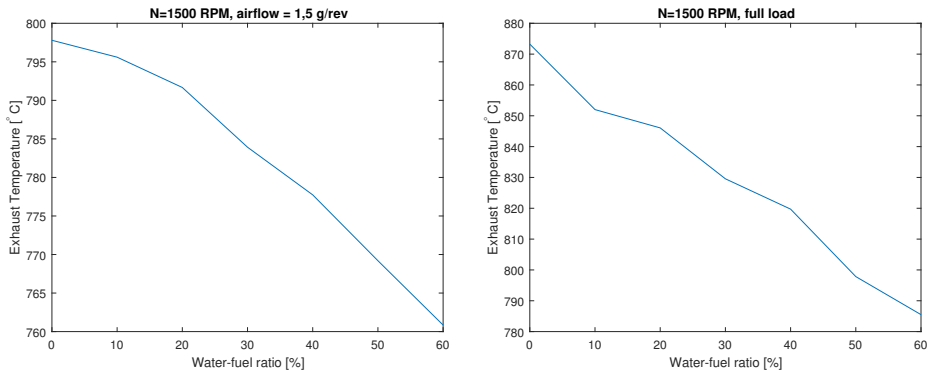


Figure 4.8: Spark retardation by the Active Knock Control at 1500 RPM, 1.5 g/rev and $\xi = 40\%$. The spark is placed at a later CA by the Active Knock Control

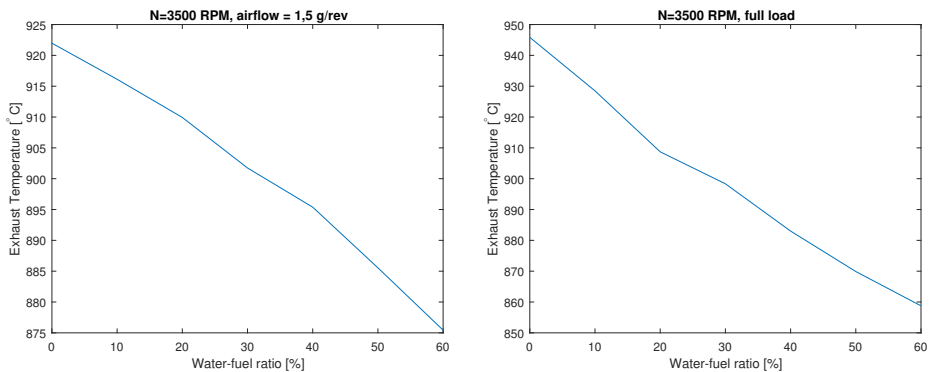
Table 4.1: Percent power increase in the operating points.

Operating point	Power increase [%]
1500 1.5 g/rev	1.6
1500 FG	3.8
2000 1.5 g/rev	2.9
2000 FG	3.5
2500 1.5 g/rev	4.0
2500 FG	9.8
3000 1.5 g/rev	1.5
3000 FG	9.8
3500 1.5 g/rev	1.4
3500 FG	5.9
4000 1.5 g/rev	0.4
4000 FG	4.7
4500 FG	2.2

To analyze the exhaust temperature, the temperature is measured just before the turbine. Figures 4.9a-d show a decrease in the exhaust temperature. This is beneficial from multiple points of view. A lower exhaust temperature decreases the wear of the turbo. In engines with an Exhaust Gas Recirculation (EGR) system, less energy is needed to cool the recirculating gases, which is beneficial from an efficiency perspective. Additionally, heat transfer losses are reduced. A lower exhaust temperature will result in a lower temperature after the compressor, due to the fact that less heat is transferred through the turbocharger.



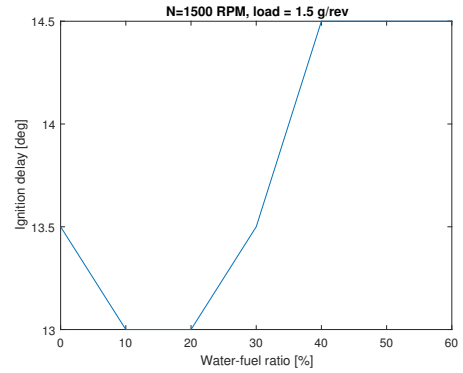
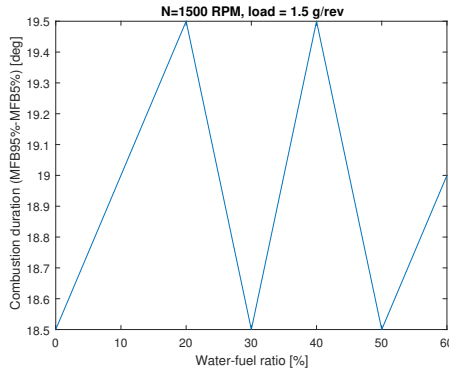
(a) Engine speed $N = 1500$ RPM, load $m = 1.5$ g/rev (b) Engine speed $N = 1500$ RPM, full load



(c) Engine speed $N = 3500$ RPM, load $m = 1.5$ g/rev (d) Engine speed $N = 3500$ RPM, full load

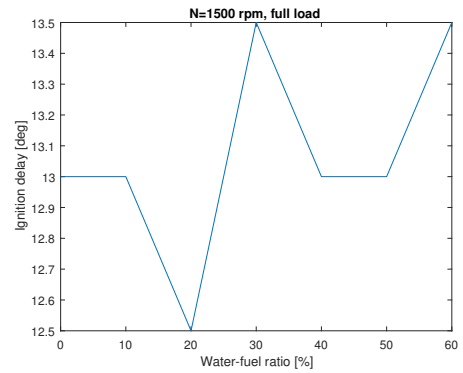
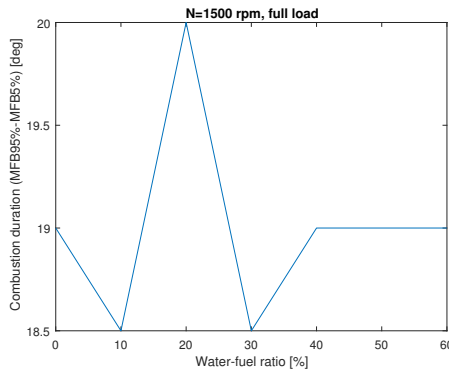
Figure 4.9: Temperature before the turbine for different water-fuel ratios

In figures 4.10a-d and 4.11a-d, the combustion duration, defined as the number of crank angles degrees between 5% MFB and 95% MFB, is calculated from the thermodynamic heat release analysis. More water does not significantly affect the combustion duration if the spark is advanced. However, assuming the ignition delay as the delay from ignition to 5% MFB, the figures show that this parameter increases with water, especially at 3500 rpm.



(a) Combustion duration, Engine speed $N = 1500$ RPM, load $m = 1.5$ g/rev

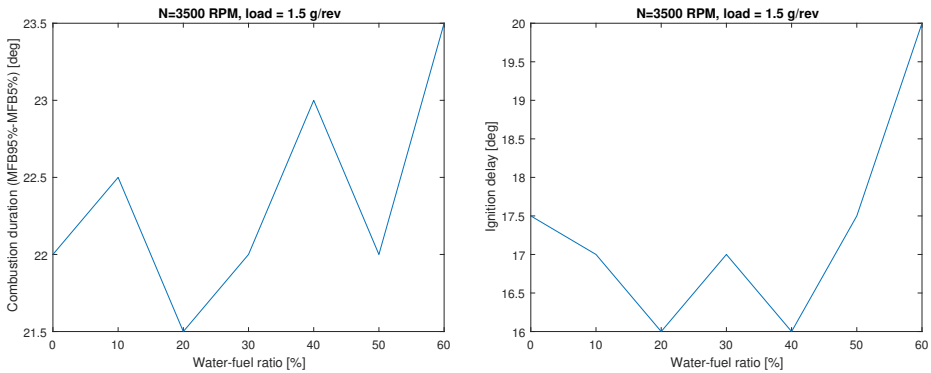
(b) Ignition delay, Engine speed $N = 1500$ RPM, load $m = 1.5$ g/rev



(c) Combustion duration, Engine speed $N = 1500$ RPM, full load

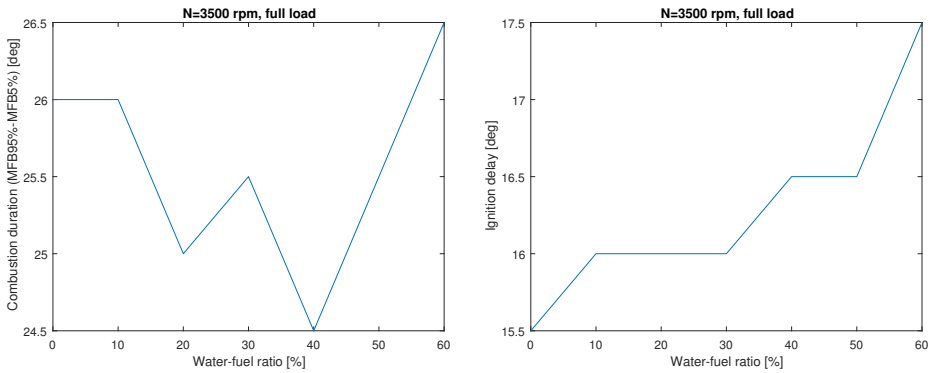
(d) Ignition delay, Engine speed $N = 1500$ RPM, full load

Figure 4.10: Combustion duration and ignition delay when injecting different amounts of water at 1500 rpm.



(a) Combustion duration, Engine speed $N = 3500$ RPM, load $m = 1.5$ g/rev

(b) Ignition delay, Engine speed $N = 3500$ RPM, load $m = 1.5$ g/rev



(c) Combustion duration, Engine speed $N = 3500$ RPM, full load

(d) Ignition delay, Engine speed $N = 3500$ RPM, full load

Figure 4.11: Combustion duration and ignition delay when injecting different amounts of water at 3500 rpm.

As explained in chapter 3, tests are made to investigate the effects of earlier water injection timing and leaner fuel injection respectively. The tests show that the cylinder pressure drops with an earlier injection. This should result in a better knock mitigation and enable even earlier ignition. Nevertheless, tests show that the ignition can not be moved earlier with earlier injection, see table B.1, appendix B. That, together with a lower pressure peak, result in lower power output than with water injected at IVO, hence water injected at IVO is the best strategy of the three. However, the test does not take changes in the exhaust into account. Note that the injection test at IVO was made with a different turbocharger (because the engine was shared with other projects), hence during different conditions, and can not directly be compared to the tests with earlier injection from a pressure perspective.

Results from the tests with λ -offset show that a water-fuel ratio of 30% usually is enough to cool the engine enough to enable λ to be increased to a value

of 1. The power output is lower than without water in all test points, and the specific fuel consumption is higher. However, the numbers might be better if the ignition is changed after λ , and in that way increase the power output. Unfortunately, this was not done in the tests. That, together with a decrease in emissions (since the catalyst is on its optimum at $\lambda=1$) might be the best way to use this technology. Additionally, tests are made to analyze the oil effects, including the water content in the oil after the injection testing. A sample of the oil was sent to the chemistry and fuel system department at Volvo Car Corporation at mid-testing. Analyzes show that there was a water content of 0.03 % in the oil. This is a surprisingly small percentage, considering about 20 litres of water was injected into the engine when the oil sample was taken. There is no way to be entirely sure why there is such a small amount of water in the oil. However, a likely explanation could be that the oil temperature was high enough to evaporate most of the water. Another possibility could be that the most of the injected water left with the exhaust, i.e. the evaporated water did not end up in the oil in the first place.

Table 4.2: Results from the oil analysis. Almost no water was found in the oil.

Petrol [%]	Heavy fractions [%]	Water [%]	Viscosity [mm^2/s]
2.5	2.7	0.03	7.94

5

Modeling

5.1 The Four-stroke Cycle

The working process of a spark ignited engine follows a four-stroke cycle, as described in [7]. The four phases are *intake*, *compression*, *expansion* and *exhaust*. At the start of the intake stroke, the inlet valve opens, usually around 10-25° BTDC, and the piston moves down towards BDC as air and fuel enters the cylinder. On the test engine in this thesis, IVO can be set between 35.5° BTDC and 14.5° ATDC. Once the piston has reached BDC and started moving upwards, the air/fuel mixture is compressed and the pressure and temperature increase. Approximately 25° BTDC, the combustion starts as the mixture is ignited by a controllable spark. The inlet valve is now closed and when the combustion is completed at around 40° ATDC, the expansion phase has already started. Unlike during the intake phase, work is produced when the gases expand. The four-stroke cycle ends through the exhaust phase, where the fluid in the chamber is pressed out through the now open exhaust valve. Worth mentioning is that the cylinder pressures during the intake and exhaust strokes are approximately equal to the intake/exhaust manifold pressures. Figure 5.1 shows the piston movement and valve positions during the four strokes.

To calculate the instantaneous volume at an arbitrary crank angle θ , some engine parameters are necessary. These are displayed in table 5.1. Insertion into equation (5.1) will provide a vector $V(\theta)$, which can be used, for example, to plot pV diagrams. The volume is also needed in the cylinder pressure model, which is presented in section 5.2. The geometrical parameters in the cylinder is graphically illustrated in Figure 5.2.

$$V(\theta) = \frac{V_d}{r_c - 1} + \frac{V_d}{2} \left(\frac{l}{a} + 1 - \cos \theta - \sqrt{\left(\frac{l}{a}\right)^2 - \sin^2 \theta} \right) \quad (5.1)$$

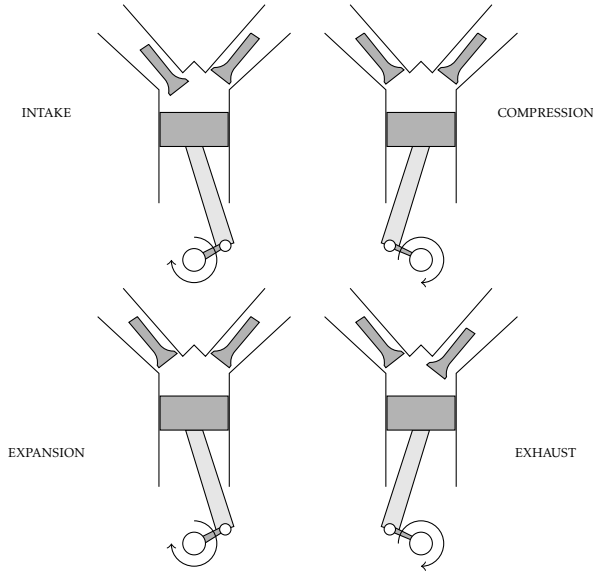


Figure 5.1: Principles of the four-stroke cycle. The intake and exhaust valves are open during the intake and exhaust parts of the cycle respectively

Note that the compression ratio is defined as the maximum cylinder volume, $V_d + V_c$, divided by the minimum cylinder volume, V_c . The stroke can be found as

$$s(\theta) = a \cos \theta + \sqrt{l^2 - a^2 \sin^2 \theta} \quad (5.2)$$

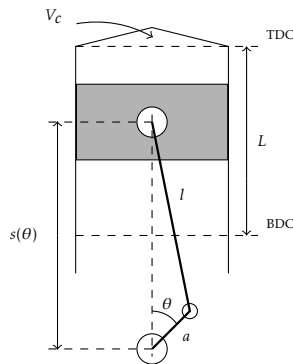


Figure 5.2: In-cylinder geometry

Table 5.1: Given engine geometry parameters

Notation	Description	Value	Unit
V_d	Displaced volume per cylinder	$4.9219 \cdot 10^{-4}$	m^3
V_c	Clearance volume per cylinder	$5.0224 \cdot 10^{-5}$	m^3
r_c	Compression ratio	10.8	–
a	Crank radius	46.6	mm
l	Connecting rod length	143.8	mm

5.2 In-cylinder Modeling

The cylinder pressure model is based on the one described in Eriksson and Andersson [6], where there are different analytic expressions for the cylinder pressure, p_{cyl} , depending on where in the cycle the process is located (i.e. depending on θ). The intake and exhaust approximations mentioned above are assumed to be valid before IVC and after EVO respectively. The final model for one cycle is displayed in equation (5.3).

$$p_{cyl} = \begin{cases} p_{im} & \theta \in [\theta_{EVC}, \theta_{int}[\\ (1 - x_i)p_{im} + x_i p_c(\theta) & \theta \in [\theta_{int}, \theta_{IVC}[\\ p_c(\theta) & \theta \in [\theta_{IVC}, \theta_{SOC}[\\ (1 - x_b(\theta))p_c(\theta) + x_b(\theta)p_e(\theta) & \theta \in [\theta_{SOC}, \theta_{EVO}[\\ (1 - x_i)p_e + x_i p_{em}(\theta) & \theta \in [\theta_{EVO}, \theta_{exh}[\\ p_{em} & \theta \in [\theta_{exh}, \theta_{IVO}[\\ (1 - x_i)p_{em} + x_i p_{im} & \theta \in [\theta_{IVO}, \theta_{EVC}[\end{cases} \quad (5.3)$$

5.2.1 Compression part

The compression part of the cycle is modeled as a polytropic process, from IVC to SOC. The relationships in equations (5.4) and (5.5) are used to model the pressure and temperature traces during the interval $\theta \in [IVC, SOC[$.

$$p_c(\theta) = p_{ivc} \left(\frac{V_{ivc}}{V(\theta)} \right)^{n_c} \quad (5.4)$$

$$T_c(\theta) = T_{ivc} \left(\frac{V_{ivc}}{V(\theta)} \right)^{n_c - 1} \quad (5.5)$$

The polytropic exponent n_c is found as the (combustion) slope in a logarithmic pV diagram. As for the pressure and temperature at IVC, these are both modeled. The initial pressure, p_{ivc} could be assumed to be equal the intake manifold pressure at IVC, $p_{im}(\theta_{ivc})$. However, if the assumption does not give sufficiently accurate results, the initial pressure can be extended to the model in equation (5.6)

$$p_{ivc} = p_{im}(\theta_{ivc}) + C_1 + C_2 \cdot N \quad (5.6)$$

where C_1 and C_2 are tuning parameters found, using for example the Least Squares Method. The initial temperature, T_{ivc} , is a bit more difficult to accurately model, since it is influenced by various parameters and occurrences. Hence, several assumptions are made. If the specific heat change between fresh air and residual gases are neglected, the initial temperature can be expressed as

$$T_{ivc} = (1 - x_r)T_{im} + x_r T_r \quad (5.7)$$

where x_r is the residual gas fraction and T_r is the residual gas temperature. The intake manifold temperature is assumed to be equal to the temperature of the fresh fluid, which is why it is used in equation (5.7). The residual gas fraction is defined as

$$x_r = \frac{m_r}{m_{tot}} \quad (5.8)$$

Here, m_{tot} is the total mass in the cylinder, including air, fuel and residual gases. With water injected, the mass of the injected water is included as well, i.e.

$$m_{tot} = m_a + m_f + m_r + m_{H_2O} \quad (5.9)$$

The residual gas fraction and temperature are determined using the ideal gas law and thermodynamic relationships for the Otto cycle. Figure 5.3 shows the ideal Otto cycle and the four states, denoted 1-4. It all sums up into four expressions, displayed in equations (5.10)-(5.13). These have to be numerically solved by an iterative algorithm, since they cannot be solved analytically. This is executed by setting an initial value of x_r , which gives initial values on the specific heat q_{in} , the temperature T_1 , and the residual gas temperature T_r . Consequently, through equation (5.10), a new value of x_r is obtained. This algorithm is repeated until x_r and T_r does not change from one iteration to another.

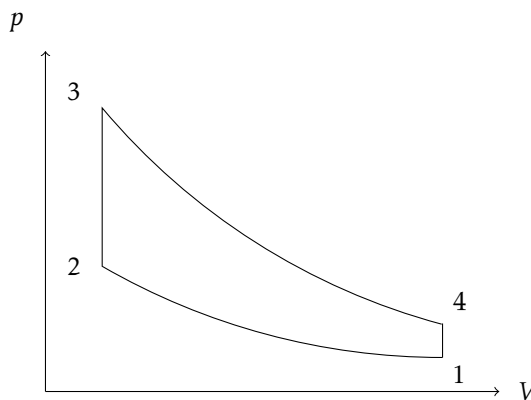


Figure 5.3: The ideal Otto cycle and its four states.

The residual gas fraction can be expressed as

$$x_r = \frac{1}{r_c} \left(\frac{p_{em}}{p_{im}} \right)^{1/\gamma} \left(1 + \frac{q_{in}}{c_v T_1 r_c^{\gamma-1}} \right)^{-1/\gamma} \quad (5.10)$$

where the specific heat, q_{in} , supplied to the system, can be calculated as

$$q_{in} = q_{LHV} \cdot \frac{1 - x_r}{1 + \lambda(A/F)_s} \quad (5.11)$$

The residual gas temperature, T_r , and temperature at state 1 in the Otto cycle, T_1 , can be found using

$$T_r = T_1 \left(1 + \frac{q_{in}}{c_v T_1 r_c^{\gamma-1}} \right) \quad (5.12)$$

and

$$T_1 = x_r T_r + (1 - x_r) T_{im} \quad (5.13)$$

The algorithm for determination of x_r , mentioned earlier, is described in detail in Appendix A.

5.2.2 Expansion part

Like the compression, the expansion part is modeled as a polytropic process, with a polytropic exponent, n_e .

$$p_e(\theta) = p_3 \left(\frac{V_3}{V(\theta)} \right)^{n_e} \quad (5.14)$$

$$T_e(\theta) = T_3 \left(\frac{V_3}{V(\theta)} \right)^{n_e-1} \quad (5.15)$$

This phase lasts from EOC to EVO, and apart from the polytropic exponent, also p_3 , V_3 and T_3 must be found to use the expressions in equations (5.14) and (5.15). The temperature at state 3 can be calculated from the temperature at SOC, as

$$T_3 = T(\theta_{SOC}) + \Delta T_{23} \quad (5.16)$$

where T_{23} is the temperature increase from state 2 to state 3 in the ideal Otto cycle and can be described

$$\Delta T_{23} = \frac{(1 - x_r) q_{LHV}}{(\lambda(A/F)_s + 1) c_v} \cdot \eta_c \quad (5.17)$$

Equation (5.17) contains the efficiency term η_c , which depends on several parameters, such as λ and injection angle.

The pressure at state 3 is given by the ideal gas law

$$p_3 = \frac{p_2}{T_2} T_3 = \frac{p(\theta_{SOC})}{T(\theta_{SOC})} T_3 \quad (5.18)$$

Assuming an isochoric combustion, the volume at state 3 is equal to the volume in state 2, which yields

$$V_3 = V_2 = V(\theta_{SOC}) \quad (5.19)$$

5.2.3 Combustion part

When the compression and expansion parts of the cylinder process are modeled, these can be interpolated to create the combustion part. This is done using the Vibe function, displayed in equation (5.21). In table 5.2, parameters in the Vibe function are presented. The rapid burn angle, also known as the rapid burn angle, is defined as the angle interval in which 10-90% of the mass is burned. Similarly, the flame development angle is the angle from ignition to 10% MFB, see figure 5.4.

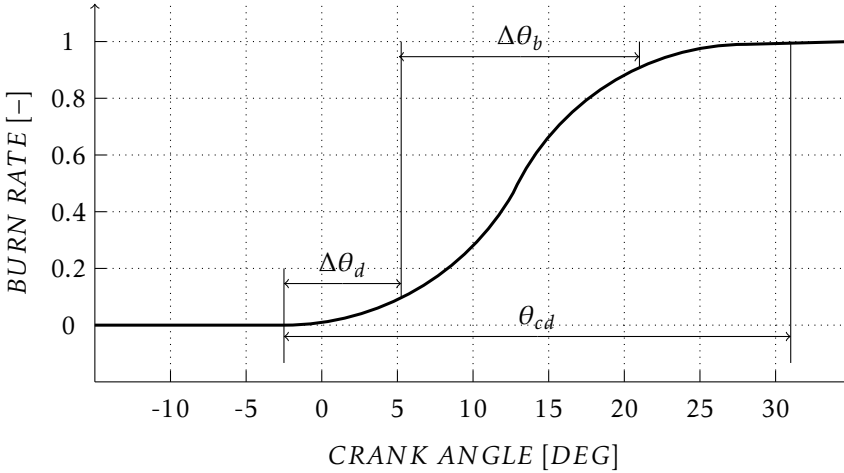


Figure 5.4: The Vibe parameters in the mass fraction burned trace. It is assumed that there is no ignition delay, i.e. the combustion starts at the ignition.

Table 5.2: Parameters in the Vibe function

Parameter	Description
θ_{SOC}	Ignition angle
θ_{cd}	Combustion duration (SOC to EOC)
$\Delta\theta_b$	Rapid burn angle
$\Delta\theta_d$	Flame development angle

A rule of thumb is that the combustion duration

$$\theta_{cd} \approx 2\Delta\theta_d + \Delta\theta_b \quad (5.20)$$

In the Vibe function, the burn rate when $\theta > \theta_{SOC}$, is expressed as

$$x_b(\theta) = 1 - e^{-a\left(\frac{\theta - \theta_{SOC}}{\theta_{cd}}\right)^{m+1}} \quad (5.21)$$

where a and m are shape factors, defined in equations (5.22a) and (5.22b).

$$a = -\ln(1 - 0.1) \left(\frac{\theta_{cd}}{\Delta\theta_d} \right)^{m+1} \quad (5.22a)$$

$$m = \frac{\ln\left(\frac{\ln(1-0.1)}{\ln(1-0.9)}\right)}{(\ln(\Delta\theta_d) - \ln(\Delta\theta_d + \Delta\theta_b))} - 1 \quad (5.22b)$$

To get an adequate Vibe function, the rapid burn angle, flame development angle and the combustion duration must be determined. Since the Vibe function is over-parametrized, θ_{cd} is assumed to always follow the relationship in equation (5.20).

With the burn rate, the expression for the cylinder pressure is interpolated from the two pressure asymptotes.

$$p(\theta) = (1 - x_b(\theta)) \cdot p_c(\theta) + x_b(\theta) \cdot p_e(\theta) \quad (5.23)$$

This equation will be used to model the cylinder pressure from SOC to EVO.

5.2.4 Valve Model

When the valves open and close, some pressure changes will occur. At some crank angle θ_{int} , the cylinder pressure will start to rise from the intake manifold pressure. Similarly, the cylinder pressure will reach the exhaust manifold pressure at a crank angle θ_{exh} after the exhaust valve is opened. This can be modeled as a cosine interpolation function.

$$x_i = \begin{cases} 0.5 \left(1 - \cos\left(\pi \frac{\theta - \theta_{int}}{\theta_{IVC} - \theta_{int}}\right) \right), & \theta \in [\theta_{int}, \theta_{IVC}] \\ 0.5 \left(1 - \cos\left(\pi \frac{\theta - \theta_{EVO}}{\theta_{exh} - \theta_{EVO}}\right) \right), & \theta \in [\theta_{EVO}, \theta_{exh}] \end{cases} \quad (5.24)$$

5.2.5 Parameter Estimation

The parameters that is estimated is shown in table 5.3. By setting each parameter to an initial value, an initial cylinder pressure trace can be obtained. This means that there now exists both a modeled and measured cylinder pressure trace. To get an accurate model, the error between the two needs to be minimized. The MATLAB solver `lsqnonlin` calculates the parameters, gathered in a vector \bar{x} , such that the optimized parameters for a certain operating point

$$\bar{x}^* = \arg \min_{\bar{x}} \sum_{k=1}^n f_k(x)^2$$

where $f_k(x)$ is the difference between the measured and modeled cylinder pressure in each sample k . This will provide an optimized cylinder pressure trace.

Table 5.3: Estimated parameters in the cylinder pressure model

Parameter	Description
$\Delta\theta_b$	Rapid burn angle
$\Delta\theta_d$	Flame development angle
n_c	Combustion polytropic exponent
n_e	Expansion polytropic exponent
η_c	Efficiency term
C_1	IVC pressure parameter
C_2	IVC pressure parameter
θ_{int}	Intake valve model angle
θ_{exh}	Exhaust valve model angle
T_{im}	Intake manifold temperature

5.3 Heat Release Analysis

To validate the Vibe function, a heat-release analysis is performed using the Rassweiler-Withrow model. The burn rate is calculated under the assumption that the mass burn rate is proportional to the pressure increase during the combustion, i.e.

$$x_{b,RW}(i) = \frac{m_b(i)}{m_{b,tot}} = \frac{\sum_{k=0}^i \Delta p_c(k)}{\sum_{k=0}^n \Delta p_c(k)} \quad (5.25)$$

Here, n is the total number of samples. The combustion pressure difference, Δp_c , is calculated as

$$\Delta p_c(i) = p_{i+1} - p_i \left(\frac{V_i}{V_{i+1}} \right)^\kappa \quad (5.26)$$

Here, p and V are the measured cylinder pressures and volumes in each sample i . For simplicity reasons, the polytropic exponent κ is assumed to be 1.3. Since the Rassweiler Withrow model is a fairly simple model, a more extensive heat release analysis is made, using the first law of thermodynamics

$$dQ_{ch} = dU + dW + dQ_{ht} \quad (5.27)$$

where dQ_{ch} is the heat release rate, dW is the work produced, dU is the internal energy rate and dQ_{ht} is the heat transfer rate. As seen in figure 5.5, a large part of the heat release rate comes from internal energy.

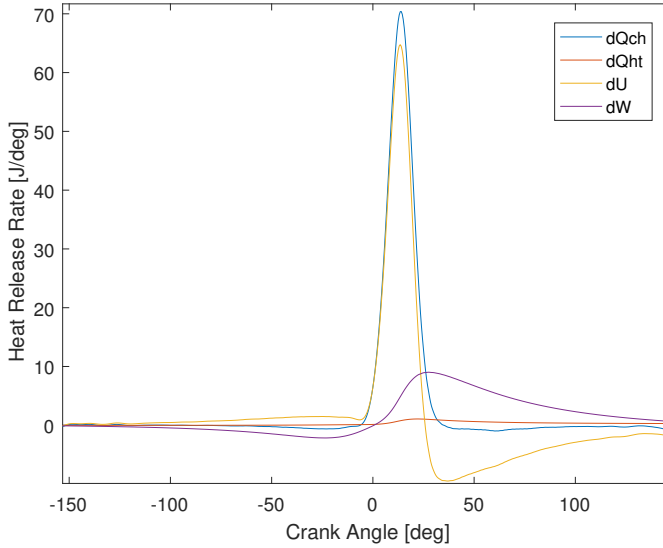


Figure 5.5: Examples of how dQ_{ch} , dU , dW and dQ_{ht} change from IVC to EVO.

The burn rate can be expressed from this as

$$x_{b,HR} = \frac{Q_{ch}}{\max Q_{ch}} \quad (5.28)$$

The work produced is the integral of the pV diagram, $dW = pdV$. The change in internal energy will depend on the cylinder temperature change, dT and the specific heat, c_v , and can be described as

$$dU = mc_v dT \quad (5.29)$$

where

$$dT = \frac{1}{m \cdot R} (pdV + VdP) \quad (5.30)$$

R is the specific gas constant, defined as the difference between the specific heats at constant pressure (c_p) and constant volume (c_v). This parameter is set to $R = 287 \text{ J}/(\text{Kg} \cdot \text{K})$. A constant could also be used for the specific heat. However, since it is a temperature dependent parameter, the following numerical model, obtained by Volvo Cars, is used instead.

$$c_v(T) = 1000(0.7 + 0.255T \cdot 10^{-3}) \quad (5.31)$$

For the cylinder temperature, T , a simple model is used, with IVC as a reference point. The temperature at IVC is assumed to be 330 K.

$$T = T_{IVC} \cdot \frac{pV}{p_{IVC}V_{IVC}} \quad (5.32)$$

To capture heat losses, Woschni's heat transfer correlation is used. The heat transfer rate is described as Newton's law of cooling,

$$\dot{Q} = h_c A (T - T_w) \quad (5.33)$$

which in the crank angle domain results in

$$dQ_{ht} = \frac{1}{6N} h_c A (T - T_w) \quad (5.34)$$

where the wall temperature, T_w , is set to a constant, $T_w = 440$ K. The parameter A is the surface area of the body in contact with the gas mixture in the cylinder. With the definition of the stroke in equation (5.2), B as the cylinder bore and parameters defined in figure 5.2, the area can be determined as

$$A = \pi B \left(\frac{B}{2} + l + a - s(\theta) + \frac{L}{r_c - 1} \right) \quad (5.35)$$

The heat transfer coefficient, h_c , can be modeled in different ways. In this thesis, a relationship from Klein [15] is used. It can be written as

$$h_c = \frac{0.013 p^{0.8} \left(c_1 \cdot \frac{2aN}{60} + c_2 \frac{(p-p_0) T_{IVC} V}{p_{IVC} V_{IVC}} \right)^{0.8}}{T^{0.55} B^{0.2}} \quad (5.36)$$

Here, p_0 is the motored pressure, assumed to follow a polytropic process at IVC,

$$p_0 = p_{IVC} \left(\frac{V_{IVC}}{V} \right)^k \quad (5.37)$$

The parameters c_1 and c_2 are cycle dependent numerical parameters,

$$c_1 = \begin{cases} 6.18, & \theta < IVC \\ 2.28, & \theta \geq IVC \end{cases} \quad (5.38)$$

$$c_2 = \begin{cases} 0, & \theta < \theta_{SOC} \\ 0.00324, & \theta \geq \theta_{SOC} \end{cases} \quad (5.39)$$

5.4 Burn Angle Model

With a working cylinder pressure model, the behavior of the rapid burn angle and flame development angle can be modeled and implemented into the pressure model. Since water injection leads to a slower combustion, the burn angles could be expressed as functions of the water-fuel ratio, ξ . Test data show a somewhat linear increase in both of the two burn angles when ξ increases for a constant ignition angle. Therefore, it is assumed that they can be expressed as linear functions of ξ . Tests also indicate that $\Delta\theta_d$ and $\Delta\theta_b$ are both speed and load dependent. Hence, the model in (5.40) is created.

$$\Delta\theta_d(\xi, m, N) = K_{1,d} \cdot \xi + K_{2,d} \quad (5.40a)$$

$$\Delta\theta_b(\xi, m, N) = K_{1,b} \cdot \xi + K_{2,b} \quad (5.40b)$$

where the load- and speed dependent K constants are modeled as

$$\begin{cases} K_{1,d} = C_{1,d} + C_{2,d} \cdot N + C_{3,d} \cdot m \\ K_{2,d} = C_{4,d} + C_{5,d} \cdot N + C_{6,d} \cdot m \\ K_{1,b} = C_{1,b} + C_{2,b} \cdot N + C_{3,b} \cdot m \\ K_{2,b} = C_{4,b} + C_{5,b} \cdot N + C_{6,b} \cdot m \end{cases} \quad (5.41)$$

The C constants are found using the least square method. To obtain these without having to validate against the same data set, the experiment data is divided into modeling- and validation data. The cylinder pressure are measured during a known number of cycles, whereupon the first half of the cycles are used as modeling data, and the second half is used as validation data. For simplicity reasons, only the operating points where $N \leq 3500$ rpm was used to determine the constants, since the points above 3500 rpm only include water-fuel ratios up to 40 %. Instead of using MATLAB to optimize the burn angles, the model can be used in the existing cylinder pressure model. After calculating the constants, equation (5.41) is written

$$\begin{cases} K_{1,d} = -2.963 + 76.7 \cdot 10^{-3} \cdot N + 1.119 \cdot 10^3 \cdot m \\ K_{2,d} = 8.417 + 85.3 \cdot 10^{-3} \cdot N + 1.087 \cdot 10^3 \cdot m \\ K_{1,b} = 2.179 + 43.7 \cdot 10^{-3} \cdot N + 0.587 \cdot 10^3 \cdot m \\ K_{2,b} = 6.212 + 0.115 \cdot N + 1.937 \cdot 10^3 \cdot m \end{cases} \quad (5.42)$$

where the engine speed N is in rps and m in kg/cycle. If optimal ignition is embedded into the burn angle model, the constants obviously change and the equation becomes

$$\begin{cases} K_{1,d} = -1.491 + 79.1 \cdot 10^{-3} \cdot N - 0.580 \cdot 10^3 \cdot m \\ K_{2,d} = 14.14 + 66.2 \cdot 10^{-3} \cdot N - 0.048 \cdot 10^3 \cdot m \\ K_{1,b} = 0.467 - 0.006 \cdot N + 0.337 \cdot 10^3 \cdot m \\ K_{2,b} = 13.05 + 0.104 \cdot N + 0.787 \cdot 10^3 \cdot m \end{cases} \quad (5.43)$$

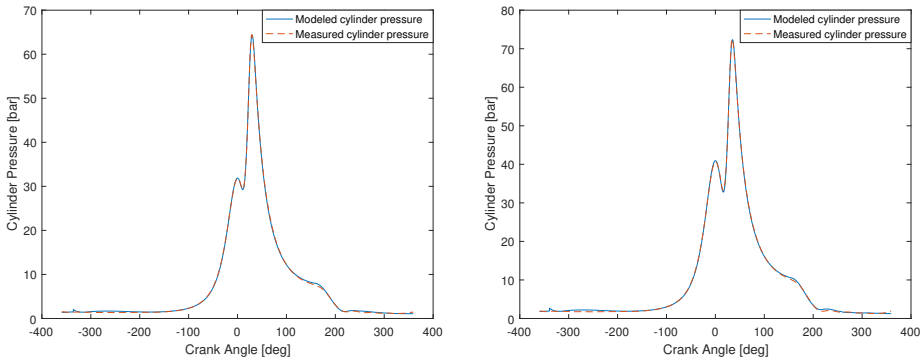
Previous research have shown that the burn angles strongly depends on the ignition angle. In Eriksson [5], the burn angles are modeled as second order polynomials with respect to the ignition angle. Some modeling are made in Soltic [23] as well.

5.5 Model Validation

To validate the cylinder pressure model, the model is compared to measured cylinder pressure data. Figures 5.6 and 5.7 show the modeled and measured cylinder pressure traces at different operating points. The model can follow measured traces during different operating conditions where the pressure behaves differently. Figures 5.8 and 5.9 show how well the cylinder pressure model can estimate the burning process in the cylinder, compared to the two heat release traces calculated as described in section 5.3. The absolute error between the Vibe function and the heat release traces are smaller in the case of the thermodynamic heat release model. The thermodynamic heat release model, unlike the Rassweiler Withrow model, takes internal energy and heat transfer losses into account. Because of this, it is assumed that it better resembles the reality. Note that the absolute error between a model, \hat{X} , and measured data, X is calculated as

$$error = \frac{|X - \hat{X}|}{X} \quad (5.44)$$

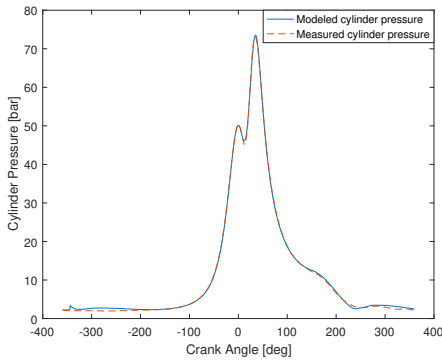
In this thesis, the model fit is defined as the mean value of equation (5.44).



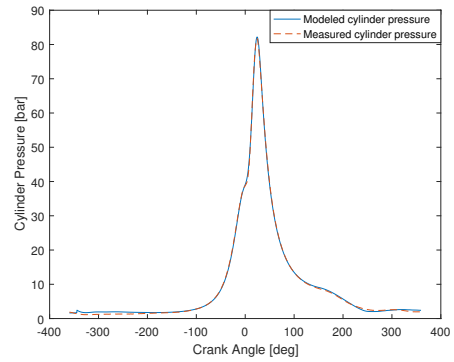
(a) Engine speed $N = 1500 \text{ rpm}$,
Torque $Tq = 255 \text{ Nm}$

(b) Engine speed $N = 1500 \text{ rpm}$,
Torque $Tq = 315 \text{ Nm}$

Figure 5.6: Cylinder pressure model in relation to the measured cylinder pressure trace in different operating points. 255 Nm corresponds to an air flow of approximately 1.5 g/rev. The validation shows a good fit at different speeds and loads.

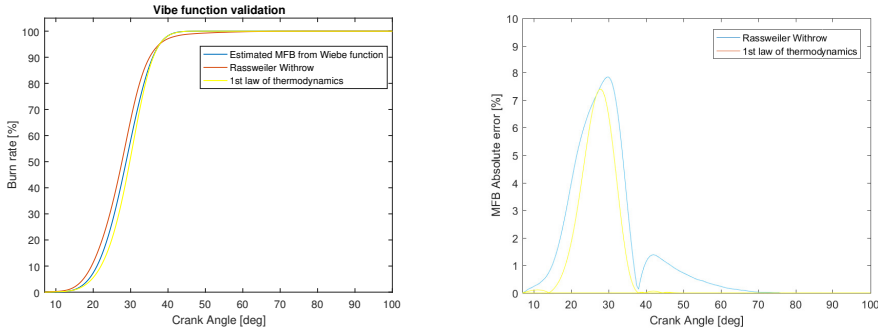


(a) Engine speed $N = 3500$ rpm,
Torque $T_q = 330$ Nm



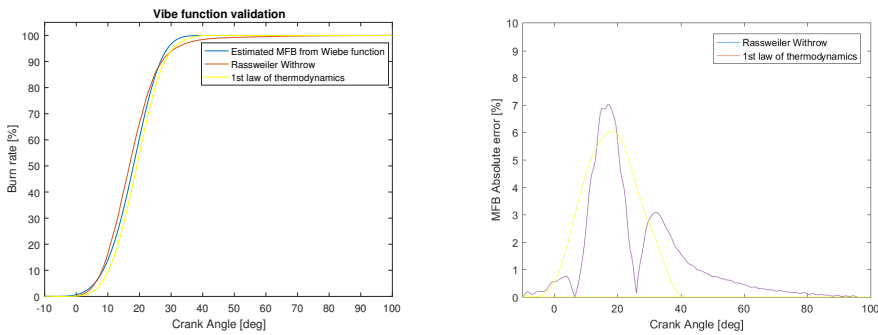
(b) Engine speed $N = 4500$ rpm,
Torque $T_q = 265$ Nm

Figure 5.7: Cylinder pressure model in relation to the measured cylinder pressure trace in different operating points. 265 Nm corresponds to an air flow of approximately 1.5 g/rev. The validation shows also here a good fit at different speeds and loads.



(a) Vibe function in the cylinder pressure (b) Absolute error between Vibe function and the heat release traces.

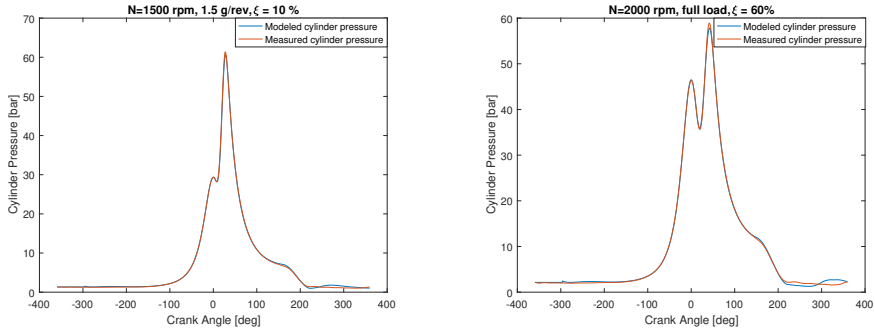
Figure 5.8: Engine speed $N = 1500 \text{ rpm}$, Torque $Tq = 315 \text{ Nm}$



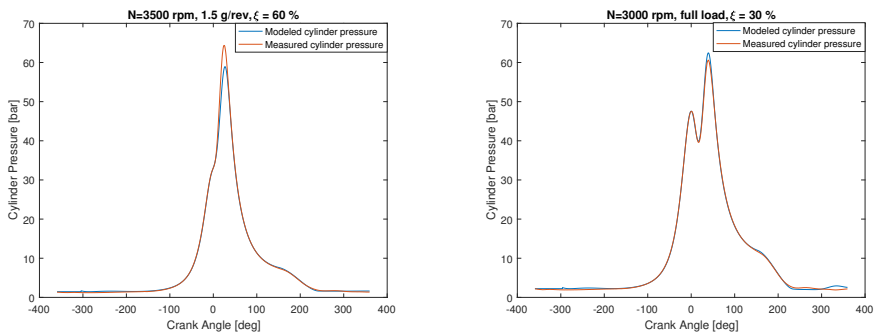
(a) Vibe function in the cylinder pressure (b) Absolute error between Vibe function and the heat release traces.

Figure 5.9: Engine speed $N = 4500 \text{ rpm}$, Torque $Tq = 265 \text{ Nm}$

Figures 5.10a-d show four different cylinder pressure validation plots when the burn angle model is used in the cylinder pressure model. The model is decent, however it seems like it in general works better with lower water amounts. Additionally, the model fit is calculated as the mean absolute error between IVC and EVO (the most interesting interval in this thesis work) and lies around 97-99 % in most cases. In the operating points where $N \geq 4000 \text{ rpm}$, no tests were made for water amounts of $\xi > 40\%$. As mentioned earlier, these points were not used to model the data. To see how well the model works outside the engine speed interval in which it was created, validations are made for these points as well. Figures 5.11 a-b still show relatively good results, only the pressure peak is a bit off. More figures can be seen in Appendix C.

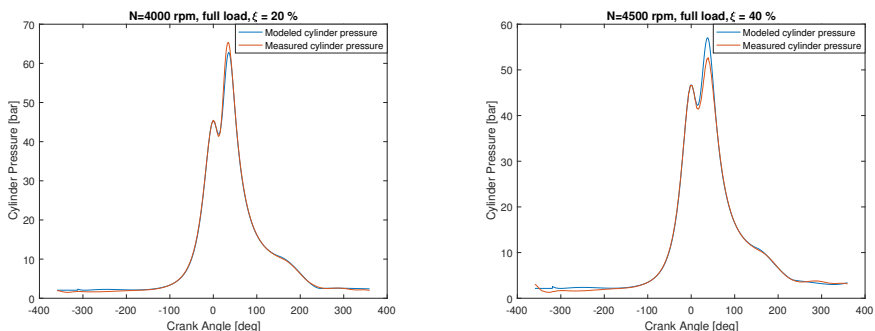


(a) $N=1500$ rpm, load = 1.5 g/rev. Model fit (b) $N=2000$ rpm, full load. Model fit 98.9 % 98.5 %.



(c) $N=3500$ rpm, load = 1.5 g/rev. Model fit (d) $N=3000$ rpm, full load. Model fit 98.7 % 97.6 %.

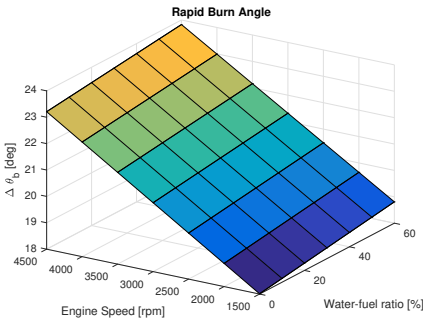
Figure 5.10: Cylinder pressure model when using modeled, instead of optimized burn angles.



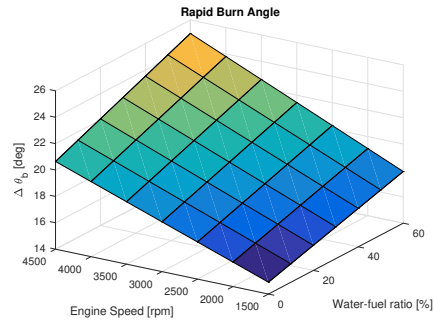
(a) $N=4000$ rpm, full load. Model fit 98.5 % (b) $N=4500$ rpm, full load. Model fit 98.2 %.

Figure 5.11: Cylinder pressure model when using modeled, instead of optimized burn angles, when engine speed is outside the engine speed modeling data interval.

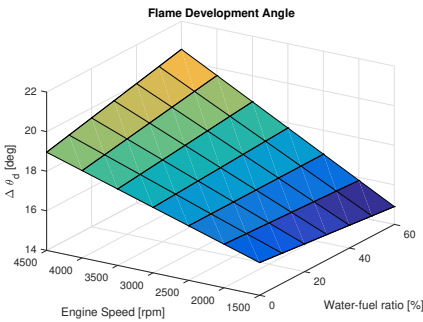
The surface plots in figure 5.12a-d show how the modeled rapid burn angle and flame development angle change with engine speed and water-fuel ratio. The rapid burn angle clearly increases with ξ when the ignition is not offset, which coincides with the results from chapter 4, where it was stated that the duration would increase if water injection is used without advancing the ignition. Moreover, the rapid burn angle slightly increases with the water-fuel ratio if the ignition is offset, which is somewhat reasonable as there was no distinct water dependency found in this case. The flame development angle increases with the water amount as well, with the exception of an engine speed at 1500 rpm.



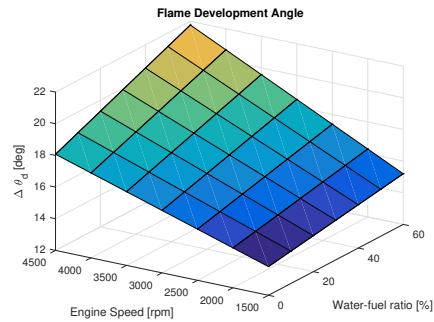
(a) Modeled $\Delta\theta_b$ in different operating points



(b) Modeled $\Delta\theta_b$ in different operating points without ignition offset



(c) Modeled $\Delta\theta_d$ in different operating points



(d) Modeled $\Delta\theta_d$ in different operating points without ignition offset

Figure 5.12: How the modeled rapid burn angle and flame development angle change with engine speed and water-fuel ratio at 1.5 g/rev.

6

Conclusions

Water injection has shown to be an efficient method to cool the engine and decrease the risk of engine knock. As shown in the results in figures 4.1-4.4, the pressure peak drops with an increase in water. This leads to a mitigation of knock and a lower power output from the engine. However, the mitigation of knock enables an earlier ignition. In table B.1, appendix B, one can see that for every 10% increase in water, the ignition can be moved approximately 1° . With a more aggressive ignition timing comes a higher pressure peak and a higher power output. Figure 4.7 shows how the power output changes with the maximum amount of water and ignition timing offset. In table 4.1 one can see the percentage power increase. Overall, the power output is increased more in high-load points which can be explained by a more cautious ignition strategy in these points.

The results show the effects with a maximum water-fuel ratio of 60% since the authors did not want to risk to destroy the engine using more water. The result clearly show that the efficiency is increased with an increase in water so it would be interesting to see what the efficiency increase would be with even higher amounts of water. The results from the oil analysis indicates that a higher water-fuel ratio could be used without having to worry too much about oil dilution.

As seen in figure 4.9, the temperature before the turbine is decreased approximately 100°C with water. A lower temperature is good for the turbine and the catalyst since the wear is increased with the temperature. There is also the possibility to cool the cylinder with water instead of cooling it with fuel, which can improve the fuel economy. This is also proven in the tests.

The Vibe burn angle model, created from the Vibe function to describe the combustion without ignition offset, has a good model fit. It shows an increase in both the rapid burn angle and flame development angle, when the water amount increases. At the same time, the heat release analysis demonstrates no correlation between combustion duration (5% MFB to 95 % MFB) if the spark is advanced.

This indicates that the spark advance accelerates the combustion process again. The ignition delay is increased in both the case with and without ignition offset. This seems reasonable, as the ignition ability of the engine should not be depending on the ignition timing. As stated, the burn angles are both dependent on the ignition angle. However, to include the ignition angle in the model, more tests would have to be done, where the ignition angle is changed in every operating point. Unfortunately, there was no time to do this.

As seen in figure 5.8, the Vibe function and the heat release trace do not match perfectly, since the Vibe function was created to match the pressure model to the measured cylinder pressure trace, rather than just the heat release trace.

There is a small error in the amount of water that was injected during the testing that need to be considered when analyzing the data. The water pump delivered a constant, non-controllable pressure and the look-up table in the injector control was created using a single fixed pump pressure difference of 3.5 bar. At higher loads, the pressure difference slightly increased, which presumably led to errors in the injection times in those operating points. A common value of the pressure difference was 4 bar which gives a difference of 0.5 bar. Equation 6.1 is describing the flow through a valve.

$$\dot{m} = C_q A \sqrt{2\rho\Delta p} \quad (6.1)$$

Equation 6.2 is showing how big the difference is in water injected for the case with a pressure difference of 4 bar. This means that for 10% the actual amount 10.7%, for 20% it is 21.4% and so on. Since every step in the tests are 10% big, the authors believe that the error is neglectable.

$$\Delta\dot{m} = \frac{C_q A \sqrt{2\rho \cdot 4}}{C_q A \sqrt{2\rho \cdot 3.5}} = 6.9\% \quad (6.2)$$

6.1 Future Work

In the future, more test data from more operating points would probably result in more accurate models. Another aspect regarding water injection to consider is the water replenishment. To make the technology more attractive, a solution that eliminates the need for refilling a water tank. In Sun et al. [24], Exhaust Water Recovery (EWR) is considered as a way to internally refill the water injection supply system. Not only would this make things easier for the customer, it also enables use of smaller tanks.

As stated in chapter 3 the best strategy might be to inject the maximum amount of water possible, increase λ to a value of 1 and the offset the ignition as early as possible. This might give the best of two worlds - higher power and less emissions. This need to be investigated further.

In this thesis, only static measurements are performed in the test bench. A continuation of this would be to do dynamic measurements and test the behavior in transients, for example, when the engine is accelerating.

Another interesting analyze would be to include the results in a vehicle simulation to see how the overall efficiency of the car changes. Since the water injection system adds weight and takes up space, the efficiency would be slightly decreased from that point of view.

Ideas of future investigations and models that could be developed include

- Investigations regarding the possibility to estimate the amount of water that is evaporated and the amount of water diluted in the oil.
- Water dependent temperature models, e.g. exhaust temperature.
- Emission tests.
- Combined λ - and ignition offset tests, where the ignition is offset at the water-fuel ratio that enables λ to be 1.
- Combine the model from this thesis with and model that predicts knock enabling prediction of possible power gain without physical testing.
- Additional water-based models to add to the cylinder pressure model

Appendix

A

Algorithm to determine residual gas fraction

Here, the algorithm to determine the residual gas fraction, x_r , is described. The equations are described in chapter 5 and down below.

$$x_r = \frac{1}{r_c} \left(\frac{p_{em}}{p_{im}} \right)^{1/\gamma} \left(1 + \frac{q_{in}}{c_v T_1 r_c^{\gamma-1}} \right)^{-1/\gamma} \quad (\text{A.1})$$

$$q_{in} = q_{LHV} \cdot \frac{1 - x_r}{1 + \lambda(A/F)_s} \quad (\text{A.2})$$

$$T_r = T_1 \left(1 + \frac{q_{in}}{c_v T_1 r_c^{\gamma-1}} \right) \quad (\text{A.3})$$

$$T_1 = x_r T_r + (1 - x_r) T_{im} \quad (\text{A.4})$$

- Set $x_r(0) = 0$ and $T_r(0) = 0 \implies q_{in}(0) = \frac{q_{LHV}}{1 + \lambda(A/F)_s}$ and $T_1(0) = T_{im}$
- Iteration i now gives:

$$q_{in}(i) = q_{LHV} \cdot \frac{1 - x_r(i-1)}{1 + \lambda(A/F)_s}$$
$$T_1(i) = x_r(i-1) T_r(i-1) + (1 - x_r(i-1)) T_{im}$$
$$T_r(i) = T_1(i) \left(1 + \frac{q_{in}(i)}{c_v T_1(i) r_c^{\gamma-1}} \right)$$
$$x_r(i) = \frac{1}{r_c} \left(\frac{p_{em}}{p_{im}} \right)^{1/\gamma} \left(1 + \frac{q_{in}(i)}{c_v T_1(i) r_c^{\gamma-1}} \right)^{-1/\gamma}$$

- Repeat until $x_r(i) = x_r(i-1)$ and $T_r(i) = T_r(i-1)$

B

Ignition Offset Results

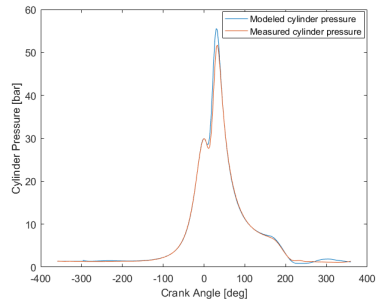
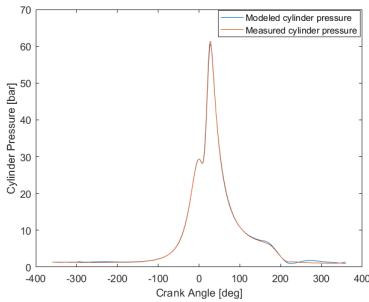
Table B.1: How many crank angle degrees the spark can be advanced in a specific operating point with a certain water amount, according to the tests. Note that the timing results are from 1500 rpm at full load.

O.P	$\xi =$	0%	10%	20%	30%	40%	50%	60%	70%
1500/1.5	0	1	1	2	3	4	4.5	5	
1500/full	0	2	2	3.5	4	5	5.5	6.5	
2000/1.5	0	1	2	3	4	4	5	6	
2000/full	0	2	3	4	4	6	6.5	7	
2500/1.5	0	1.5	2.5	4	5	6.5	7.5	-	
2500/full	0	5	6	7	8	8	9	-	
3000/1.5	0	2	3	4	5.5	6.5	8	-	
3000/full	0	4	6	7	8.5	9	10	-	
3500/1.5	0	1	2	3	4	5	7	-	
3500/full	0	3	5	6	7.5	8.5	10	-	
4000/1.5	0	0	2	3.5	5	-	-	-	
4000/full	0	4	6	7.5	-	-	-	-	
4500/full	0	0	1	4	6	-	-	-	
Injection timing	$\xi =$	0%	10%	20%	30%	40%	50%	60%	
IVO		0	2	2	3.5	4	5	5.5	
50° before IVO		0	1	2	3	4	5	6	
100° before IVO		0	1	2	3	4	5	6	

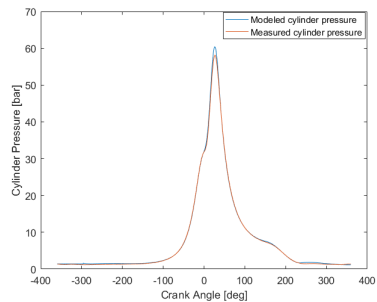
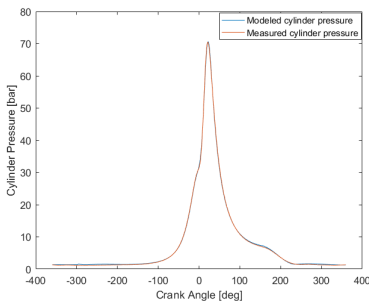
C

Burn Angle Model

Additional results from the burn angle modeling.

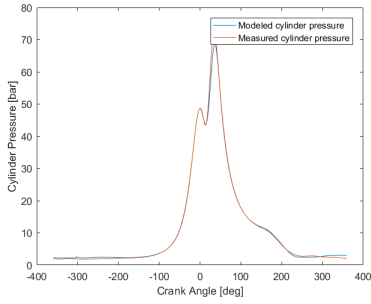


(a) $N=1500$ rpm, load = 1.5 g/rev. $\xi = 10$ %. (b) $N=1500$ rpm, load = 1.5 g/rev. $\xi = 60$ %.

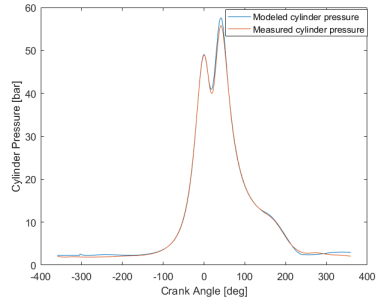


(c) $N=3000$ rpm, load = 1.5 g/rev. $\xi = 10$ %. (d) $N=3000$ rpm, load = 1.5 g/rev. $\xi = 60$ %.

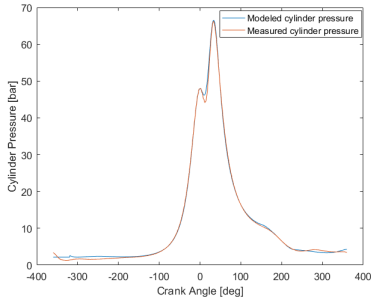
Figure C.1: Cylinder pressure model when using modeled, instead of optimized burn angles (1500 and 3000 rpm).



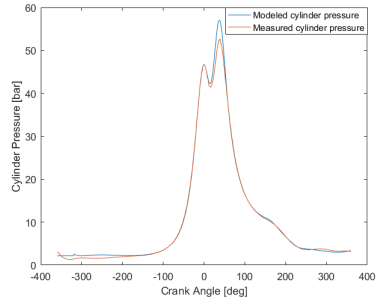
(a) $N=3500$ rpm, full load. $\xi = 10\%$.



(b) $N=3500$ rpm, full load. $\xi = 60\%$.



(c) $N=4500$ rpm, full load. $\xi = 10\%$.



(d) $N=4500$ rpm, full load. $\xi = 40\%$.

Figure C.2: Cylinder pressure model when using modeled, instead of optimized burn angles (3500 and 4500 rpm).

Bibliography

- [1] ACEA. Real driving emissions test. URL <http://www.acea.be/industry-topics/tag/category/real-driving-emissions-test>. Cited on page 1.
- [2] Meghraj Bhagat, Khanh Cung, Jaclyn Johnson, Seong-Young Lee, Jeffrey Naber, and Sam Barros. Experimental and numerical study of water spray injection at engine-relevant condition. *SAE Technical Paper 2013-01-0250*, 2013. doi:10.4271/2013-01-0250. Cited on page 5.
- [3] Alberto Boretti. Water injection in directly injected turbocharged spark ignition engines. *Applied Thermal Engineering* 52 (2013) 62-68, 2012. URL https://ac.els-cdn.com/S1359431112007296/1-s2.0-S1359431112007296-main.pdf?_tid=4d7f6530-081a-11e8-87c4-00000aab0f01&acdnat=1517577158_512f05c55a900e98fe76cac90ae146ce. Cited on page 6.
- [4] Lindsay Brooke, Stuart Birch, Kami Buchholz, and Paul Weissler. New engines 2016. *SAE International*, 2016. Cited on page 1.
- [5] Lars Eriksson. *Spark Advance Modeling and Control*. PhD thesis, Linköping University, Linköping, 1999. URL http://www.fs.isy.liu.se/en/Publications/PhD/99_PhD_580_LE.pdf. Dissertation No. 580. Cited on pages 3 and 37.
- [6] Lars Eriksson and Ingemar Andersson. An analytic model for cylinder pressure in a four stroke si engine. *SAE Technical Paper 2002-01-0371*, 2002. URL <https://saemobilus.sae.org/content/2002-01-0371>. Cited on pages 3 and 29.
- [7] Lars Eriksson and Lars Nielsen. *Modeling and Control of Engines and Drivelines*. John Wiley & Sons, Ltd, 2014. Cited on pages 3, 4, 11, and 27.
- [8] Lars Eriksson and Martin Sivertsson. Calculation of optimal heat release rates under constrained conditions. *SAE Int. J. Engines* 9(2):2016, 2016. doi:10.4271/2016-01-0812. Cited on page 4.

- [9] Le-zhong Fu, Zhijun Wu, Liguang Li, and Xiao Yu. Effects of water injection temperature on characteristics of combustion and emissions for internal combustion rankine cycle engine. *SAE Technical Paper 2014-01-2600*, 2014. doi:10.4271/2014-01-2600. Cited on page 5.
- [10] Per Ganestam. Empirical knock model for automatic engine calibration. Master's thesis, Lund University, SE-221 00 Lund, Sweden, 2010. Cited on page 4.
- [11] Mohit Hashemzadeh Nayeri. Cylinder-by-cylinder torque model of an si-engine for real-time applications. Master's thesis, Linköping University, SE-581 83 Linköping, 2005. Cited on page 4.
- [12] John B. Heywood. *Internal Combustion Engine Fundamentals*. McGraw-Hill Education, 1988. Cited on pages 3 and 4.
- [13] Fabian Hoppe, Matthias Thewes, Henning Baumgarten, and Jürgen Dohmen. Water injection for gasoline engines: Potentials, challenges, and solutions. *International Journal of Engine Research*, 2016. Cited on pages 4 and 5.
- [14] Arturo Iacobacci, Luca Marchitto, and Gerardo Valentino. Water injection to enhance performance and emissions of a turbocharged gasoline engine under high load condition. *SAE Int. J. Engines 10(3):2017*, 2017. doi:10.4271/2017-01-0660. Cited on pages 4, 5, and 6.
- [15] Markus Klein. *Single-zone Cylinder Pressure Modeling and Estimation for Heat Release Analysis of SI Engines*. PhD thesis, Linköping University, Linköping, 2007. URL <http://www.diva-portal.org/smash/get/diva2:24199/FULLTEXT01.pdf>. Dissertation No. 1124. Cited on pages 3 and 36.
- [16] R. Lanzafame. Water injection effects in a single-cylinder cfr engine. *SAE Technical Paper 1999-01-0568*, 1999. URL <https://saemobilus.sae.org/content/1999-01-0568>. Cited on page 5.
- [17] R. Lanzafame and S. Brusca. Evaluation of the effects of water injection in a single cylinder cfr engine. *SAE Technical Paper 2001-01-1212*, 2001. URL <https://saemobilus.sae.org/content/2001-01-1212>. Cited on page 5.
- [18] Fu Lezhong, Wu Zhijun, Yu Xiao, Deng Jun, Hu Zongjie, and Li Liguang. Experimental investigation of combustion and emission characteristics for internal combustion rankine cycle engine under different water injection laws. *Energy Procedia 66 (2015) 89 – 92*, 2015. Cited on pages 4 and 5.
- [19] Niclas Lindström. A framework for evaluation of cylinder balancing controllers. Master's thesis, Linköping University, SE-581 83 Linköping, 2017. Cited on page 4.

- [20] Wei Mingrui, Nguyen Thanh Sa, Richard Fiifi Turkson, Liu Jinping, and Guanlun Guo. Water injection for higher engine performance and lower emissions. *Journal of the Energy Institute* 90 (2017) 285-299, 2015. Cited on page 5.
- [21] Achint Rohit, Sridev Satpathy, Jeongyong Choi, John Hoard, Gopichandra Surnilla, and Mohannad Hakeem. Literature survey of water injection benefits on boosted spark ignited engines. *SAE Technical Paper 2017-01-0658*, 2017. doi:10.4271/2017-01-0658. Cited on pages 4, 5, and 6.
- [22] Yaojung Shiao and John J. Moskwa. Cylinder pressure and combustion heat release estimation for si engine diagnostics using nonlinear sliding observers. *IEEE Transactions on Control Systems Technology*, 1995. Cited on page 4.
- [23] Patrik Soltic. *Part-Load Optimized SI Engine Systems*. PhD thesis, Swiss Federal Institute of Technology, Zürich, 2000. URL <https://doi.org/10.3929/ethz-a-004089317>. Dissertation ETH No 13942. Cited on page 37.
- [24] Yong Sun, Michael Fischer, Michael Bradford, Adam Kotrba, and Eric Randolph. Water recovery from gasoline engine exhaust for water injection. *SAE Technical Paper 2018-01-0369*, 2018. doi:10.4271/2018-01-0369. Cited on page 44.
- [25] Jeremy Worm, Jeffrey Naber, Joel Duncan, Sam Barros, and William Atkinson. Water injection as an enabler for increased efficiency at high-load in a direct injected, boosted, si engine. *SAE Int. J. Engines* 10(3):2017, 2017. doi:10.4271/2017-01-0663. Cited on pages 4 and 6.